

PHOTOMETRIC AND POLARIMETRIC OPPOSITION PHENOMENA EXHIBITED BY SOLAR SYSTEM BODIES

VERA ROSENBUSH,¹ NIKOLAI KISELEV,² VICTOR
AVRAMCHUK,¹ AND MICHAEL MISHCHENKO³

¹*Main Astronomical Observatory of the National Academy of
Sciences, 27 Zabolotny Street, 03680 Kyiv, Ukraine*

²*Institute of Astronomy, Kharkiv National University,
35 Sumskaya Street, 61022 Kharkiv, Ukraine*

³*Goddard Institute for Space Studies, 2880 Broadway,
New York, NY 10025, USA*

Abstract. Ground-based and spacecraft observations of atmosphereless solar system bodies (planets, satellites, planetary rings, and asteroids) and cometary and interplanetary dust particles have provided a wealth of new photometric and polarimetric data over a wide range of phase angles and wavelengths. This chapter reviews the progress in the study of the photometric and polarimetric phase effects observed near opposition. We also present the results of recent polarimetric observations of the Galilean satellites of Jupiter, Iapetus, and the asteroid 64 Angelina at very small phase angles. Analyses of the available data allow us to determine the parameters of the brightness and polarization opposition effects and investigate correlations between them. The results obtained may form the observational basis for detailed theoretical modeling and interpretation of the phase effects.

1. Introduction

Measurements of the intensity and polarization of scattered light as functions of the phase angle are a primary source of information about the physical properties of the surfaces of solar system bodies. Such observations are especially informative near the opposition, i.e., at small phase angles. Many atmosphereless solar system bodies (ASSBs) exhibit an opposition brightening, the so-called brightness opposition effect (BOE), as a nonlinear brightness increase toward smaller phase angles. Negative values of the degree of linear polarization at

In G. Videen and M. Kocifaj (eds.), *Optics of Cosmic Dust*
(Kluwer Academic Publishers, Dordrecht, 2002), pp. 191-224

backscattering angles are also a common property of rather different objects such as asteroids, satellites, planets, comets, interplanetary dust particles, and planetary rings. Both effects have also been observed for many laboratory samples [1].

A number of physical mechanisms have been proposed to explain the photometric opposition effect and negative polarization resulting from the interaction of light with porous, powder-like surface layers or rough surfaces of the ASSBs [2–5]. Presently, the so-called coherent backscattering mechanism (CBM) and the mutual shadowing mechanism (SM) are believed to be the primary candidates to explain the observed opposition phenomena. Both astronomical observations of ASSBs and laboratory measurements of structural analogs of planetary regoliths may provide important tests of theoretical models.

Until now, the origin of the BOE and negative polarization is not yet fully understood, the lack of high-accuracy photometric and polarimetric data for various objects at small phase angles being one of the main reasons. Observations at the smallest phase angles ($\leq 2^\circ$) are very rare. Furthermore, the polarization at these angles is often weak (several tenths of a percent), thereby necessitating very high measurement accuracy and making most of the available data poorly suitable for studies of the opposition effects.

This chapter covers three closely related subjects: (i) a brief review of the existing photometric and polarimetric data for ASSBs at small phase angles; (ii) a more detailed discussion of most recent polarimetric observations at phase angles approaching zero; and (iii) a discussion of how to determine the parameters of the BOE and negative polarization and study their relationships.

2. Basic definitions

In this chapter, we use the standard photometric and polarimetric terminology adopted in planetary astrophysics. The opposition region is defined as the range of phase angles from about 25° down to 0° . The phase angle, α , is the angular distance between the Sun and the observer as seen from the astronomical object.

Usually, the BOE means a nonlinear surge in brightness, measured either in magnitude scale (m) units or in intensity (I) units, at small phase angles. For several high-albedo objects, the BOE is observed in the form of a very sharp and narrow intensity peak often called the opposition spike. For phase angles $\alpha_{\text{opp}} < \alpha \leq 25^\circ$, the brightness, measured in magnitudes, increases linearly with decreasing phase angle, where α_{opp} is the phase angle at which the BOE begins. The curves showing the dependence of the distance-corrected brightness on the phase angle are called photometric phase curves. The slope of the linear part of the phase curve is called the phase coefficient: $\beta = dm/d\alpha$.

For the quantitative description of the BOE, the following parameters are useful: the amplitude Δm (or the enhancement factor ζ) and the half-width at half-

maximum HWHM_B of the opposition surge; the background intensity I_b calculated by extrapolating the brightness linearly to zero phase angle; β ; and α_{opp} . There are two definitions of the amplitude of the BOE. The first one is the ratio of two intensities, $I(\alpha_1)/I(\alpha_2)$, where $0 \leq \alpha_1 \leq \alpha_2 \leq \alpha_{\text{opp}}$. This definition is often used for the quantitative description of the BOE when the lack of observations does not allow one to plot a detailed phase curve. The second one is the brightness increase relative to I_b . In theoretical studies of the BOE, the enhancement factor ζ is usually defined as the ratio of the backscattered intensity at exactly the backscattering direction to the background intensity.

Unpolarized light scattered by a particulate surface becomes partially linearly polarized. By definition, the degree of linear polarization is $P = (I_{\perp} - I_{\parallel}) / (I_{\perp} + I_{\parallel})$, where I_{\perp} and I_{\parallel} are the intensity components with the electric vectors perpendicular and parallel to the scattering plane. The latter is defined by the Sun, the observer, and the object. The polarization degree changes with phase angle and produces a specific so-called polarization phase curve $P(\alpha)$. It often has a negative branch ($I_{\perp} < I_{\parallel}$) near opposition and a positive branch ($I_{\perp} > I_{\parallel}$) at phase angles $\alpha > \alpha_{\text{inv}}$. Angle α_{inv} is called the inversion angle and is the phase angle at which the polarization changes sign ($I_{\perp} \approx I_{\parallel}$). The parameters of the negative polarization branch are α_{inv} , P_{min} (the minimal polarization value), and α_{min} (the phase angle of minimal polarization). We also use the parameter $0 < \text{HWHM}_p < \alpha_{\text{min}}$, specifying the phase angle at which the polarization value is equal to $\frac{1}{2} P_{\text{min}}$. All these parameters depend on the physical and chemical characteristics of the scattering particles and on the macroscopic roughness profile of the particulate surface.

The behavior of the negative polarization branch at backscattering angles ($\alpha < 2^\circ$) is very intriguing and poorly understood. A very asymmetric negative branch is observed for high-albedo Saturn's rings, while the dark Moon shows a regular, nearly parabolic negative branch [6]. Mishchenko [7] introduced the term "polarization opposition effect" (POE) to indicate situations when the polarization of the backscattered light, being zero at zero phase angle, becomes negative and reaches its maximal negative value at a very small phase angle (less than 1°). He further assumed that both the extremely narrow BOE and the POE for high-albedo objects are caused by coherent backscattering. This approach implies the possible presence of a separate broad negative minimum of polarization centered at a significantly larger phase angle and generated by an optical mechanism potentially different from coherent backscattering. Therefore, the resulting polarization curve at backscattering angles can have different shape depending on the relative contributions of different mechanisms and can range from a single POE spike to a single, nearly parabolic negative polarization branch. In contrast, Shkuratov [8]

and Muinonen *et al.* [4] believe that the CBM can explain all types of negative polarization branches observed for ASSBs and interplanetary and cometary dust.

3. Observations

3.1 Limitations of photometric and polarimetric observations

The specific illumination/observation geometry often does not allow one to observe an object at both small and large phase angles. For example, the smallest accessible phase angles in ground-based observations of the Moon (outside of an eclipse) and Mars are about 0.5° and 1.2° , respectively. Furthermore, the parameters characterizing the BOE at extremely small phase angles may not be reliable because the brightness spike can be broadened due to the finite angular size of the solar disk [9], which should be taken into account for such objects as the Moon, Mars, and the satellites of Jupiter and Saturn. Ground-based observations of such distant objects as the satellites of Jupiter, Saturn, and, especially, Neptune and Uranus are quite difficult because of the narrow phase angle coverage: from 0° to 12° for Jupiter, from 0° to 6° for Saturn, from 0° to 3° for Uranus, and from 0° to 2° for Neptune. In the case of satellites rotating along low orbits such as Phobos, Deimos, Tethys, Dione, Rhea, Titania, Oberon, and others, the scattered light from the primary planet and, potentially, planetary rings can also be a major problem in obtaining precise photometric and polarimetric data.

Furthermore, the brightness and polarization of a satellite can change with orbital phase (the so-called longitude effect). This can be caused by the heterogeneity of the local albedo over the surface of the satellite. To investigate the phase dependence of the brightness and polarization, averaged measurements for the leading and the trailing hemisphere of a satellite are usually used. This averaging can lead to a significant scatter of data points. Therefore, the separation of variations caused by the longitude effect from those caused by changing solar phase angle should be done separately for each orbital longitude.

There are also brightness (and possibly polarization) variations caused by the rotation of irregularly shaped objects such as Hyperion, Nereid, and some asteroids. In such cases, the orientation of the pole, which may cause brightness variations in different apparitions, must be taken into account.

3.2 Photometric observations

The Moon. The study of the lunar disk is important, since the Moon is used as a standard for interpreting observations of other planets, satellites, and asteroids. Moreover, the disk of the Moon can be easily resolved, and the distribution of the surface brightness can be mapped as a function of the phase angle and the local angles of incidence and reflection. In fact, the majority of the photometric studies of the Moon have been done for specific small areas rather than for the whole

lunar disk.

The lunar regolith is an example of a surface that exhibits prominent backscattering. The first rather accurate phase curve of the disk-integrated intensity in the visible spectral range was obtained by Russell [10]. The most accurate dependence of the disk-integrated brightness on the phase angle was derived by Rougier [11] on the basis of photoelectric observations. The existence of the BOE was demonstrated by Gehrels *et al.* [12]. Lane and Irvine [13] observed the whole Moon in ten narrow spectral bands as well as in the UVB filters within the phase angle range 6.6° – 118.6° .

A sharp increase of brightness near opposition for 31 lunar regions was first discovered by Barabashev [14] in 1922. Many photometric observations of the lunar formations covering a wide range of wavelengths have been collected in [15–20]. These studies have established that the brightness phase curves for different surface features on the Moon behave differently depending on the location on the disk and, thus, on the structure and composition of the surface. However, all of them show a nonlinear surge in brightness near opposition. According to Gehrels *et al.* [12], there is a 10–15% increase in brightness between phase angles 1.4° and 0.7° . The total brightening within the phase angle range from 5° to 0° may reach 50%–100%. Colorimetric investigations of different lunar regions have demonstrated the spectral dependence of the BOE as well as variations of its value with surface type. An extensive review of lunar photometry performed by different authors, and its interpretation was given by Hapke [21].

Detailed investigations of the BOE were continued during the Apollo program [22–24]. Apollo 8 photographs provided the first opportunity to determine the lunar photometric function in the vicinity of zero phase without extrapolation. The opposition brightening was found to be 1.3–1.4 as the phase angle decreased from 8° to 0° . Differences in the BOE amplitude for maria (7%) and for highlands (19%) at the smallest phase angles (from 1.5° to 0°) were discovered. There was no obvious correlation between the degree of brightening and the albedo or other characteristics of surface.

Recently, observations performed during the Clementine mission have been analyzed, and the BOE was investigated in detail in the visible and near infrared spectral ranges [25–29]. According to Kreslavsky *et al.* [29], the brightness phase curves for regions in Sinus Medii and Mare Fecunditatis clearly flatten at phase angles $< 0.25^\circ$, which is due to the significant angular size of the solar disk as viewed from the Moon. The average amplitude of the lunar opposition surge in the range of phase angles from 1° to 0° is approximately 10%. There is no obvious wavelength dependence of the opposition surge for the phase angle range 0° – 1.4° .

Mercury. Danjon [30,31] performed the first reliable and detailed measurements of the phase dependence of brightness for Mercury at phase angles from 3° to 123° . The most important result of these observations is that there is a clear opposition brightness increase at phase angles less than about 12° . CCD disk-

integrated photometric data were recently obtained with the SOHO spacecraft in the phase angle ranges $2^\circ < \alpha < 22^\circ$ and $160^\circ < \alpha < 178^\circ$ [32]. The combination of these data with ground-based observations revealed that the brightness surge for Mercury exceeds 40% between phase angles 10° and 2° .

Mars. This planet is not an atmosphereless body, but the optical thickness of the Martian atmosphere during the periods of high transparency is very small. Therefore, the atmospheric effects are usually negligible in the red light ($\lambda > 500$ nm), and the light reflected by the surface is dominant. However, dust storms, which often occur near opposition, may cause a significant atmospheric scattering contribution leading to strong brightness variations. The latter can suppress or even totally obscure the BOE.

The BOE for Mars was first detected by Vaucouleurs [33,34] during the 1958 opposition and was subsequently confirmed by O'Leary [35] and Bugaenko *et al.* [36]. Extensive observations of Mars during the 1971–75 oppositions were reported by Aleksandrov *et al.* [37], who also found a brightness increase at small phase angles. The extrapolation of the observed brightness to zero phase angle yields the BOE amplitude of about 0.1–0.3^m at different wavelengths [34].

BOE measurements for different morphological formations of Mars at phase angles down to 0.1° were obtained by the Viking Orbiter 1 spacecraft [38]. A sharp brightness increase (10%) was observed at phase angles $\alpha < 3^\circ$ for flat, bright and dark areas in the Chryse Acidalia, Arabia, and Elysium Planitia regions. The opposition peak was stronger and narrower for high-albedo areas than for dark features. A weak, if any, opposition effect was found for the Syrtis Major regions. Thorpe [39] concluded that the BOE for Mars does exist and depends on the surface albedo and porosity.

The brightness increase for Pavonis Mons was measured in eight spectral bands ($\lambda = 315 - 550$ nm) using Phobos-2 observations at phase angles 0° and 15.7° [40]. The amplitude, defined as the ratio $I(0^\circ)/I(15.7^\circ)$ and determined after correcting for the atmospheric effects, was found to be about 1.7. It depended weakly on the wavelength within the spectral range $\lambda = 315-445$ nm, but decreased substantially at $\lambda = 445-550$ nm.

Satellites of Mars. Photometric data for Phobos and Deimos based on Mariner-9 observations cover a restricted range of large phase angles ($18^\circ-83^\circ$) [41]. A more extensive coverage was obtained from the Viking observations: $1.3^\circ-122^\circ$ for Phobos and $0.5^\circ-122^\circ$ for Deimos [42,43]. These data allowed, for the first time, to study the BOEs for both satellites of Mars and the wavelength dependence of the photometric phase curves between 445 nm and 593 nm. The phase curves exhibited a linear part between 20° and 80° with phase coefficients about 0.024 mag/deg for Phobos and 0.020 mag/deg for Deimos, and a conspicuous brightness surge at phase angles less than 20° . The phase curves for the Martian satellites were also compiled for phase angles up to 125° from ground-based and spacecraft

photometric observations [44]. These investigations have shown that the phase curves for Phobos and Deimos are very similar. This result contradicts previous indications that the phase curve for Phobos is steeper than that for Deimos [42].

Disk-resolved images of Phobos taken by the Phobos 2 spacecraft at phase angles less than 30° showed that rims of many grooves and craters are usually 20–30% brighter than the surrounding areas, whereas the brightness contrast is much less evident at larger phase angles [45–47]. The Phobos disk-integrated photometry with the Hubble Space Telescope (HST) at phase angles ranging from 10.6° to 40.5° allowed one to track the start of the opposition brightening [48].

Galilean satellites. All Galilean satellites of Jupiter show unequivocal BOEs [49–53]. According to [54], the amplitude of the opposition effect is 0.17^m for Io, 0.09^m for Europa, 0.07^m for Ganymede, and 0.25^m and 0.13^m for the leading and the trailing side of Callisto, respectively. Thompson and Lockwood [55] discovered an extremely narrow spike in brightness (about 0.2^m) at a phase angle $\alpha \approx 0.2^\circ$ for both hemispheres of Europa, as shown in Fig. 1a. As one can see, the photometric phase curves are essentially the same over the phase angle range 0.5°–12° for both hemispheres of Europa.

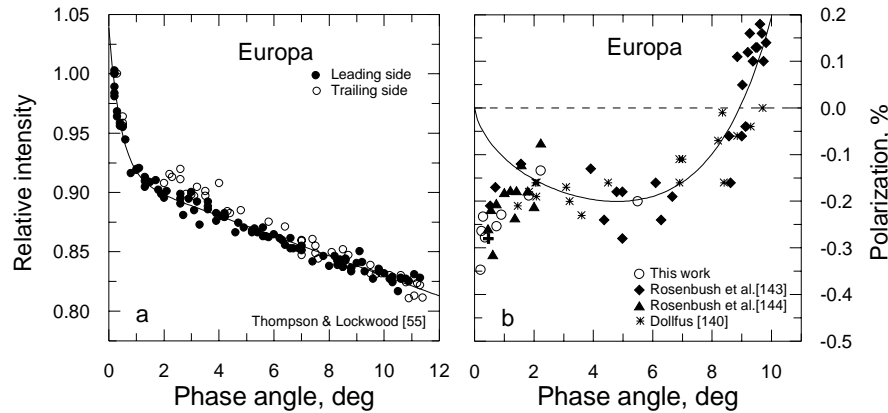


Figure 1: The brightness (a) and polarization (b) opposition effects for Europa in the V band. The brightness data are fitted with an exponential-linear function [56]; the polarization data are fitted with a trigonometric polynomial [57] (solid curves).

The leading/trailing hemisphere dichotomy for the Galilean satellites was already known from the observations of Stebbins [49] and Stebbins and Jacobsen [50]. The leading hemispheres of Io, Europa, and Ganymede are brighter than the trailing hemispheres in the entire phase angle range 0.5°–12°. For Callisto, however, the trend is reverse at large phase angles: the trailing side is brighter than the leading one (Fig. 2a). Near the opposition, there is almost no difference in the

brightness of the two sides due to the fact that the opposition surge of the dark side is much stronger than that of the bright side. Note that there is also an albedo asymmetry of the Galilean satellites in the infrared [58] and in the ultraviolet [59].

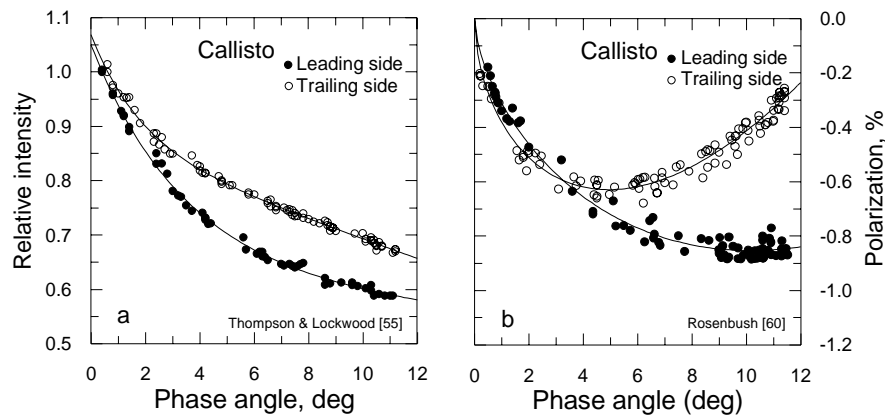


Figure 2: The BOE (a) and the negative polarization branch (b) for the leading and trailing hemispheres of Callisto in the V band. The variations of polarization with orbital longitude are taken into account [60]. The fitted functions (solid curves) are analogous to those in Fig. 1.

Systematic observations of Io showed brightness changes of up to a few percent per year not observed for the other Galilean satellites [53]. They are most likely caused by albedo changes associated with active volcanic processes. Until now, there are no carefully measured photometric phase curves for both the leading and the trailing side of Io with a good phase angle coverage near opposition and a small scatter of data points. Nevertheless, the available data allow one to conclude that despite the similar albedos for Io (0.62) and Europa (0.68), the phase coefficient for Io (0.022) is considerably greater than that for Europa (0.006) [54].

Spacecraft observations marked a new stage in the study of the Galilean satellites by extending the range of phase angles up to 160° . Domingue and Verbiscer [61] combined the results of previous telescopic observations [51,52, 62] with the Voyager data and constructed photometric phase curves for the leading and trailing hemispheres of the satellites to examine any possible hemisphere dichotomies. They have confirmed that Europa and Callisto have a strong hemisphere dichotomy in their rotational lightcurve. Ganymede has a hemisphere brightness difference in the same sense as Europa, but not as pronounced.

Studies of the BOE for several features on the surface of Europa by the Galileo spacecraft are especially interesting [63]. According to the measurements in three

spectral bands (410, 560, and 990 nm), all terrains exhibit narrow ($\text{HWHM}_b < 0.2^\circ$) BOEs, but with different amplitudes. The amplitudes for most abundant materials on Europa are about 1.5 times greater than those predicted from ground-based observations. Low-albedo materials at dark locations exhibit unusually strong opposition effects, up to four times stronger than bright icy terrains.

Satellites of Saturn. In spite of the significant volume of ground-based [64–66] and spacecraft [67–71] data, the BOEs for the satellites of Saturn are very poorly studied. The data appear to be too sparse to construct detailed photometric phase curves. Noland *et al.* [64], Franklin and Cook [65], and Franz and Millis [66] found BOEs for all satellites, although their quantitative descriptions are absent. On the basis of the available data, only the geometric albedo, phase coefficients, and brightness differences between the leading and trailing hemispheres of the inner satellites Mimas, Enceladus, Tethys, Dione, and Rhea were determined [67]. The leading hemispheres of the inner satellites Tethys, Dione, and Rhea are brighter than their trailing sides, whereas for Enceladus and Mimas an opposite trend was found. These satellites have very high geometric albedos (0.77 for Mimas, 1.04 for Enceladus, 0.80 for Tethys, 0.55 for Dione, and 0.65 for Rhea [72]), thereby indicating icy surfaces with a very low fraction of dark opaque materials. The Voyager spacecraft images have established that the surface of Enceladus is strongly backscattering with normal reflectance >1.1 , i.e., substantially greater than that of any typical natural surface such as freshly fallen snow.

Of all distant satellites of Saturn, extensive photometric data exist only for Hyperion and Iapetus. The sharp and irregular shape of Hyperion [71], probably produced by fragmentation of a larger parent body, causes its asynchronous rotation. In comparison with high-albedo inner satellites, Hyperion has low geometric albedo, which changes from 0.17 to 0.28 in line with visibility aspect. Earth-based photometric observations of this satellite in the phase angle range 0.23° – 5.90° were reported in [65,73,74]. The Voyager data [71] extended this range up to 80° . The BOE amplitude determined by Degewij *et al.* [73] is 0.38^m in the V filter. The phase coefficient determined from the spacecraft data is 0.013 ± 0.007 mag/deg.

Iapetus is known to have a very unusual brightness asymmetry between the leading (geometric albedo $p_v = 0.05$) and the trailing ($p_v = 0.60$) hemisphere [69,75]. Therefore, the linear phase coefficient strongly varies with longitude from 0.028 mag/deg for the bright side to 0.068 mag/deg for the dark side. A nonlinear surge was found for both sides of the satellite [64,65]. Ground-based [64–66,74,76,77] and spacecraft [69] data allowed one to derive the phase curves for the bright and dark sides of Iapetus at phase angles from 0.23° to 90° .

Analyses of all available data have shown that detailed photometric phase curves can be constructed only for Tethys [67,78,79], Hyperion, and Iapetus. It should be noted that the phase curves for Iapetus can be obtained only for a very

narrow range of longitudes: 270° – 300° for the bright and 80° – 92° for the dark side.

Saturn's rings. The unusual increase of brightness of the Saturn system near opposition was observed for the first time by G. Müller [80], who attributed the phenomenon to the rings and explained it by the effect of mutual shadowing among the ring particles. Using these observations, Seeliger [81] made the first quantitative determination of the opposition effect. Subsequently, Schönberg [82] and Hertzsprung [83] performed separate observations of rings A and B and studied their respective phase-angle brightness dependencies in the phase angle range from 0.12° to 6.45° . Schönberg [84] did not find any systematic features in the spectral brightness dependence of the B ring.

The work by Franklin and Cook [85] has become a classical study of the BOE. They obtained differentiated brightness curves for Saturn and for the A and B rings in the phase angle range 0.09° – 5.68° in the B and V filters. The scatter of individual data points is so small that these results can be considered standard. No significant difference between the two rings was detected.

Numerous and extensive observations were performed in order to investigate the potential dependence of the photometric phase curve for Saturn's rings on declination of the Earth with respect to the ring plane (the so-called tilt effect) and on the orbital phase angle (the azimuthal effect) at different wavelengths [86–90]. The most important results of these papers can be summarized as follows: there was no significant difference between the shape of the phase curves for the A and B rings in different spectral bands [89]; no significant distinction was found between the western and the eastern cusp of the rings [86]; the phase curves for the cusps were remarkably similar at all ring tilts, wavelengths, and radial distances from Saturn [90].

The center of Saturn is often used as a spectrophotometric standard for studying the brightness of the rings. Therefore, it is very important to investigate the intrinsic opposition effect of Saturn. Avramchuk (unpublished data) has shown that the amplitude and HWHM_B of the BOE for Saturn may reach 0.03^m and 0.49° in the V filter, respectively. The phase coefficient is found to be 0.010 mag/deg , which is smaller than that for the rings (0.037 mag/deg).

Satellites of Uranus. In 1983, Brown and Cruikshank [91] reported evidence of a strong opposition brightness surge of Ariel, Titania, Oberon, and possibly Umbriel at near-infrared wavelengths (1.43 – $2.57 \mu\text{m}$). Subsequently, Goguen *et al.* [92] performed V filter photometry of Titania and Oberon in the phase angle range $0.06^{\circ} < \alpha < 3.1^{\circ}$. It was found that the amplitudes of orbital lightcurves of satellites were less than 0.1^m . The phase coefficients for Titania and Oberon ($\beta = 0.10 \pm 0.02 \text{ mag/deg}$) were comparable with those observed for asteroids at similar phase angles. The increase of brightness was found to be 0.4^m in the phase angle range from 3.04° down to 0.06° . The measurements from Voyager and Voyager 2

extended the phase angle range up to 139° [93]. Buratti *et al.* [94] concluded that the five largest satellites of Uranus form a unique class of low-albedo, spectrally flat objects weakly different from each other. According to [95], the amplitudes of the opposition surges were very large (0.40^m – 0.75^m), with the exception of Umbriel (0.14^m).

Extensive photometric data for four Uranian rings and 16 satellites were obtained with the HST in 1997 [96,97]. The phase angle range was 0.03° – 2.8° and the 25 different filters covered the wavelength range from 0.27 to 2 μm . The data by Karkoschka [97] near $\alpha = 0^\circ$ showed phase curves much steeper than those observed previously for each satellites.

Satellites of Neptune. In spite of the narrow phase-angle coverage ($< 2^\circ$), ground-based observations of these satellites are suitable for studies of the BOE. The only satellite, for which the phase dependence of brightness has been examined in detail, is Nereid [95]. This is a small, chaotically rotating satellite with an irregular shape, which displays brightness variations at time scales from hours to days or even months [98]. The lightcurve obtained by Schaefer and Tourtellotte [95] in 1998 shows variations of up to 0.52^m with a single peak coinciding with opposition. Therefore, it is possible that this peak is mainly caused by the opposition effect. The phase curve displays an opposition brightening with an amplitude of 0.44^m , which puts Nereid in the class of objects with very strong opposition surges.

The V filter photometry of Triton [92] showed a weak brightness increase ($\beta = 0.03 \pm 0.03$ mag/deg) with an amplitude of 0.05^m .

Asteroids. Gehrels [99] was the first to observe the opposition effect for asteroids, namely, for an S-type asteroid 20 Massalia (Fig. 3a). Subsequently, Harris *et al.* [100] found an opposition spike for E-type asteroids 44 Nysa and 64 Angelina. The BOE is also typical of low-albedo asteroids [101]. At present, a significant number of photometric observations of asteroids have been published, but only a few of them have a good phase-angle coverage and are suitable for a study of the BOE [100–112]. The BOE parameters vary with taxonomic class of asteroids [113]. The average phase coefficients are 0.042, 0.033, 0.029, and 0.019 mag/deg for C-, M-, S-, and E-type asteroids, respectively [114]. The BOE typically starts at phase angles 3° – 6° [115]. There are indications that the BOE parameters can vary slightly within one type of asteroid [116].

The photometric properties of near-Earth asteroids (NEAs) are very similar to those of the main belt asteroids [117]. Specifically, S-type asteroids of both families have the same average phase coefficient $\beta = 0.030 \pm 0.007$ mag/deg. The BOE is only known for two NEAs [118,119].

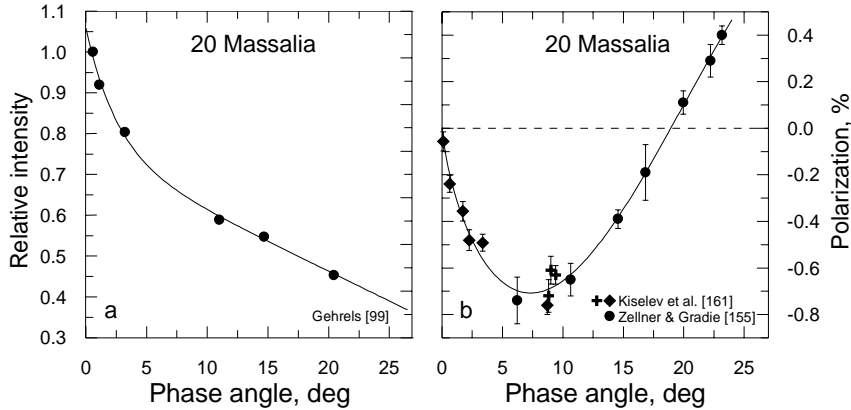


Figure 3: (a) The BOE and (b) the negative polarization branch for the S-type asteroid 20 Massalia. The fitted functions (solid curves) are analogous to those in Fig. 1.

Comets. Measurements of the brightness of cometary dust near opposition are still very rare. There is only one comet, 28P/Neujmin 1, for which photometric observations have been performed at phase angles less than 1° ($0.8^\circ < \alpha < 8^\circ$) [120]. Available observational data and their interpretation can be found in [121,122]. Schleicher *et al.* [122] indicated that the phase dependence of the comet Halley dust has a pronounced curvature over the observed range 1.5° – 66° (Fig. 4a). The phase coefficient is 0.045 mag/deg near opposition but becomes nearly flat at angles greater than about 30° . The brightness at 0° is 2.9 times that at the minimum near 50° . Fernandez *et al.* [123] determined the brightness phase dependence of the Encke nucleus. The phase coefficient is 0.06 mag/deg, thereby implying one of the steepest slopes known for any small solar system body.

Interplanetary dust. The photometric opposition effect is also observed for interplanetary dust particles (IDPs) [124]. Renard *et al.* [125] obtained the phase-angle dependence of the IDP brightness in the ecliptic plane within the phase angle range $0^\circ \leq \alpha \leq 90^\circ$ and at the solar distance 1.5 AU. According to [126,127], the decrease in brightness of the zodiacal light with increasing phase angle is of the order of 0.015 mag/deg. The enhancement factor is about 2 at phase angles below 7° .

3.3 Polarimetric observations

The Moon. Starting with Arago, polarimetric observations of the Moon have been carried out by many investigators. However, a hundred years after Arago, B. Lyot [6] discovered that the disk-integrated polarization of the Moon as well as that of its local regions becomes negative at phase angles about 23° . Detailed reviews of

the polarimetric properties of the Moon can be found in [20,128–131]. Summarizing these studies, one can conclude that the main properties of the negative polarization branch for the Moon are the following: i) the negative polarization branch for the whole Moon is almost symmetric with parameters $P_{\min} = -1.2\%$, $\alpha_{\min} = 11^\circ$, and $\alpha_{\text{inv}} = 23.6^\circ$; ii) the lunar objects of different morphology exhibit different values of P_{\min} within the range from -0.6% to -1.4% . The low negative polarization values are characteristic of bright highlands, whereas dark maria have greater $|P_{\min}|$; iii) the dependence of P_{\min} on the surface albedo for various lunar formations has a horse-shoe shape: at low albedos, $|P_{\min}|$ increases with albedo, but then decreases when the albedo exceeds a certain threshold; iv) the absolute value of P_{\min} for bright craters is independent of the wavelength, but slightly increases with wavelength for dark material; iv) the inversion angle slightly increases with wavelength.

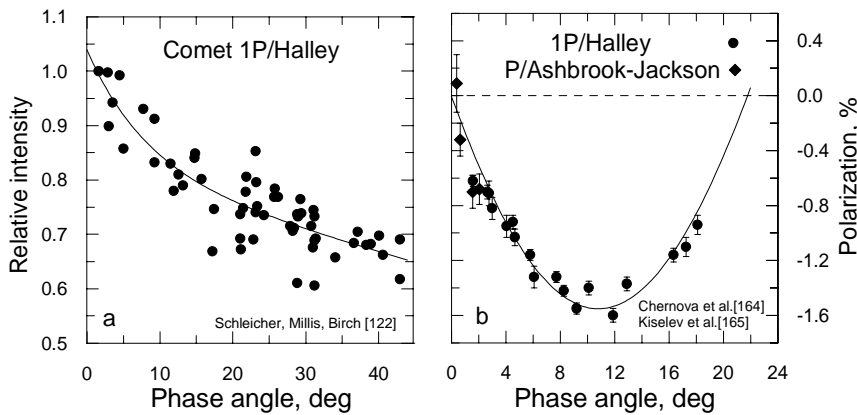


Figure 4: The BOE (a) and negative polarization branch (b) for comet 1P/Halley. The fitted functions (solid curves) are analogous to those in Fig. 1.

Mercury. The first observations of Mercury near opposition ($5^\circ < \alpha < 22^\circ$) were made by Lyot [132] in 1930. The disk-integrated polarization was very similar to that for the waxing and waning Moon. Dollfus and Auriete [133] extended the polarization curve for Mercury down to the phase angle 4° in several spectral bands. They confirmed that the polarization parameters for Mercury, $P_{\min} = -1.4\%$, $\alpha_{\min} = 11^\circ$, and $\alpha_{\text{inv}} = 25^\circ$, were close to those of the Moon.

Mars. Initially Lyot [6] and later Dollfus [134], Dollfus and Focas [135], Morozhenko [136], and Bugaenko *et al.* [137] measured polarization of the whole Mars as well as of different regions near opposition. The results can be summarized as follows: i) the polarization curves are different for different oppositions; ii) P_{\min} is about -1% and α_{\min} is about 12° ; iii) the inversion angle

increases with wavelength and is in the range 24° – 29° . Thus, the inversion angle for Mars is among the largest values ever measured for ASSBs; iv) the absolute value of the degree of polarization is greater for dark features (maria) than for bright features (continents); v) the degree of polarization of the dark features strongly depends on the latitude and season.

Deimos. Zellner [138] discovered a well-developed negative polarization branch for Deimos, with P_{\min} close to -1.5% , α_{\min} close to 10° , and an inversion angle of about 19.5° .

Galilean satellites. Several polarimetric data sets for the Galilean satellites have been obtained with UBVR filters at phase angles ranging from 11.8° to nearly 0° [139–144]. The phase-angle, orbital, and spectral dependencies of polarization were studied. There are some systematic differences in the depth of the negative polarization branch for Io, Europa, Ganymede, and Callisto. Large orbital variations in the degree of polarization were found for Callisto (Fig. 2b) and Io, whereas smaller longitudinal effects have been detected for Ganymede and Europa. The minimal polarization values for the trailing hemispheres of Io, Europa, and Ganymede are systematically higher than those for the respective leading hemispheres. However, the leading hemisphere of Callisto is characterized by considerably higher values of polarization and larger α_{\min} in all spectral bands as compared to those for the trailing hemisphere. The separation of the phase and longitudinal effects in polarization was performed for Ganymede [140] and Callisto [140, 60].

For the first time, the presence of the polarization opposition effect in the form of a sharp spike of negative polarization centered at a very small phase angle of $\alpha \approx 0.5^{\circ}$ – 0.7° and superimposed on the regular negative polarization branch was detected for Io, Europa, and Ganymede [143–145]. This phase angle is comparable to the width of the brightness peak observed for Europa (Fig. 1b), thereby indicating that both opposition phenomena are likely to be produced by the coherent backscattering mechanism [143]. For Callisto, a sharp negative polarization spike at $\alpha < 1^{\circ}$ was not detected (Fig. 2b).

Satellites of Saturn. There are sparse polarization measurements for three satellites of Saturn: Dione, Rhea, and Iapetus [146,147]. The results are sufficient to estimate the depth of the negative polarization branch, but the phase-angle dependence of polarization cannot be determined. Dione and Rhea have similar values of P_{\min} close to -0.4% . For Iapetus, the negative branch was found to be much deeper for the dark leading hemisphere ($P_{\min} = -1.3\%$) than for the bright trailing side ($P_{\min} = -0.2\%$).

Saturn's rings. Lyot [4] measured polarization of Saturn's rings A and B at very small phase angles. The polarization curve for the B ring was found to be highly asymmetric and differed dramatically from the nearly parabolic negative

polarization branch typical of most ASSBs. Extensive investigations of the ring polarization were also performed in [148–151]. Johnson *et al.* [150] measured a detailed profile of negative polarization for the A and B rings before and after opposition in the phase angle range 0.5° – 6° . The $P(\alpha)$ curve was asymmetric with $P_{\min} = -0.5\%$ at a phase angle of about 3° . They called the extrapolated sharp change of polarization at very small phase angles ($0^\circ < \alpha < 0.5^\circ$) “the hypothesized polarimetric opposition effect.” Johnson *et al.* concluded that both the BOE and the POE are caused by light-scattering processes that occur within optically active regolith layers of individual ring particles and are not due to multiple reflections of light and mutual shadowing by different particles.

Dollfus [151] indicated that the observed polarization appears to be the result of several effects. He corrected the polarimetric measurements of the rings for the effect of illumination from the Saturn’s globe and for the multiply scattered component and derived the polarization curve of the B ring caused by direct reflection of sunlight by the ring particles. In his original work Dollfus [151] approximated the polarization curve $P(\alpha)$ by an asymmetric curve with $P_{\min} \approx -0.35\%$ at $\alpha_{\min} \approx 2^\circ$. Later, Dollfus re-analyzed those data and found a narrow spike of negative polarization centered at a phase angle $\alpha \approx 0.5^\circ$ [143]. Thus, the POE, which was first unequivocally detected for the Galilean satellites, was also observed for the Saturn’s B ring.

Asteroids. Lyot [152] was the first to discover polarization of light scattered by asteroids. He found that asteroids 1 Ceres and 4 Vesta exhibit the same negative polarization at small phase angles as the Moon, Mars, and Mercury. An extensive program of polarimetric observations has been carried out by Zellner, Gradie, and Gehrels [153–155]. As a result, the negative polarization branch for many asteroids was studied in detail. The parameters P_{\min} , α_{\min} , and α_{inv} , were found to be different between the main composition types of asteroids S, C, M, and E.

Polarimetric studies of asteroids were actively pursued in the former Soviet Union [156] and, in recent years, were continued in the Kharkiv National University [157]. The main purpose of this research was to classify asteroids according to their P_{\min} values and to study the spectral dependence of P_{\min} . It has been found that the absolute value of P_{\min} increases with wavelength for moderate-albedo asteroids (types S, M, and V), whereas P_{\min} of low-albedo asteroids (types G, B, CP, and F) decreases with wavelength. Several asteroids have been observed near opposition ($0.1^\circ < \alpha < 3.3^\circ$) [158–161]. However, only the observations of 20 Massalia allow one to investigate the behavior of polarization near opposition in detail. All available data for Massalia are shown in Fig. 3b. Obviously, the negative polarization branch is slightly asymmetric and has no peculiarities at very small phase angles.

Comets. Negative polarization of sunlight scattered by cometary dust was discovered by Kiselev and Chernova [162,163] in 1976 and is a typical feature of

comets. 1P/Halley is a unique comet for which the detailed negative branch of polarization was observed with high accuracy at phase angles down to 1.57° [164]. It has a symmetric shape with $P_{\min} = -1.5\%$ and $\alpha_{\min} = 11^\circ$ in the green continuum filter. Only one comet, 47P/Ashbrook-Jackson, was observed at smaller phase angles down to 0.36° [165]. The polarization phase curves for the comets Halley and Ashbrook-Jackson are plotted in Fig. 4b. There is possibly a small depression of polarization at a phase angle about 2° .

Interplanetary dust. Polarization observations of the zodiacal light have been performed by various authors. Wolstencroft and Rose [166] detected negative polarization near opposition with P_{\min} close to -2% , which is similar to the values observed for comets. However, the inversion angle was only of the order of 12° , i.e., significantly smaller than that for comets. Thus, one should not exclude the possibility that physical properties of interplanetary dust particles are not identical to those of cometary dust [167,168].

4. Recent polarimetry of satellites and an asteroid

As we could see from our review of polarimetric observations of ASSBs, the measurements at very small phase angles ($\alpha < 1^\circ$) are rare, and the detailed behavior of polarization is still poorly known. Below we present and discuss the results of the most recent polarization observations of the Galilean satellites, Iapetus, and the asteroid 64 Angelina near opposition. These high-albedo objects were specifically selected for a study of the POE. For some of them (Europa and 64 Angelina), a spike-like BOE is also found. This is in agreement with the theoretical prediction by Mishchenko [7], according to which the POE and the sharp BOE can be two spectacular manifestations of the same optical phenomenon, viz., coherent backscattering.

Galilean satellites. CCD imaging polarimetry of the Galilean satellites was carried out with the 70-cm telescope of the Astronomical Observatory of the Kharkiv National University during the period 9–25 September 1998 over the phase angle range $0.4^\circ - 3^\circ$ in the V filter [144,169]. During the 2000 opposition, electrophotopolarimetric observations of the Galilean satellites were performed with the same telescope in the UBVR filters [145]. The minimal phase angle reached was as small as 0.20° . For the first time, the polarization phase dependence for the Galilean satellites near opposition was studied in detail and with high accuracy (about $\pm 0.02\%$). Figures 5a and 5b illustrate the behavior of polarization for Europa (before and after the opposition) and Ganymede in different spectral bands. As one can see, there is a sharp spike of negative polarization for Europa (with an amplitude of 0.35% at a phase angle of 0.20°). The angular profile of the observed polarization feature resembles the theoretical angular profile caused by the CBM for nonabsorbing Rayleigh particles [7,170]

and the profile measured for a particulate surface composed of microscopic MgO grains [6]. Similar results were obtained in the laboratory for other high-albedo fine powder samples [1]. The behavior of polarization for Ganymede near opposition is significantly different from that for Europa. The POE may be in the form of either a well-separated peak or a highly asymmetric curve. However, previous observations indicate the likely superposition of a separate narrow peak ($P_{\min} = -0.38\%$ and $\alpha_{\min} = 0.6^\circ$) and a regular negative branch.

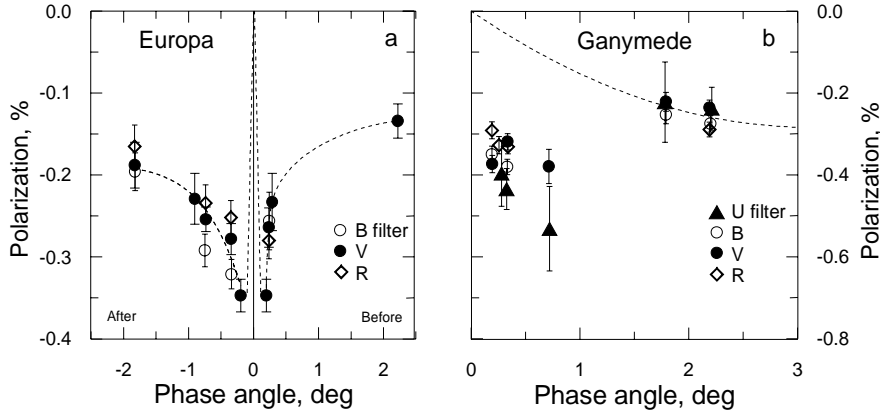


Figure 5: The polarization opposition effect for Europa (a) and Ganymede (b) in the UBVR filters. The dashed curve for Ganymede is a trigonometric fit of all previous observations [140–144].

The results of all polarization measurements for Europa obtained by different observers [140–144] are summarized in Fig. 1b. The analysis of the available data shows that Io, Europa, and Ganymede have a sharp spike of negative polarization centered at a very small phase angle ($< 1^\circ$) and superimposed on the regular negative polarization branch. It is interesting that the satellites demonstrate spikes of different shape. Callisto (Fig. 2b) exhibits only the regular negative polarization branch for the leading hemisphere and a slightly asymmetric phase curve for the trailing hemisphere without any features near opposition [60].

Iapetus. Observations of Iapetus were carried out with the five-channel UBVR photopolarimeter installed on the 1.25-m telescope of the Crimean Astrophysical Observatory [137]. Iapetus was observed from 11 October 1998 to 18 January 1999 at phase angles up to 6.1° . The minimal phase angle reached was as small as 0.30° . The phase-angle dependence of polarization for the leading (dark) and trailing (bright) hemispheres of Iapetus is shown in Fig. 6. The phase curve for the dark side (Fig. 6a) is asymmetric with $P_{\min} = -1.1\%$ at $\alpha_{\min} = 3.5^\circ$ and does not show the POE. The bright side (Fig. 6b) reveals a high degree of negative polarization (up to -0.8% at $\alpha = 1^\circ$); whereas, polarization is approximately

–0.2% at phase angles 5° – 6° . One may expect that the negative polarization branch for the bright side of Iapetus either contains a separate POE peak or is a highly asymmetric curve.

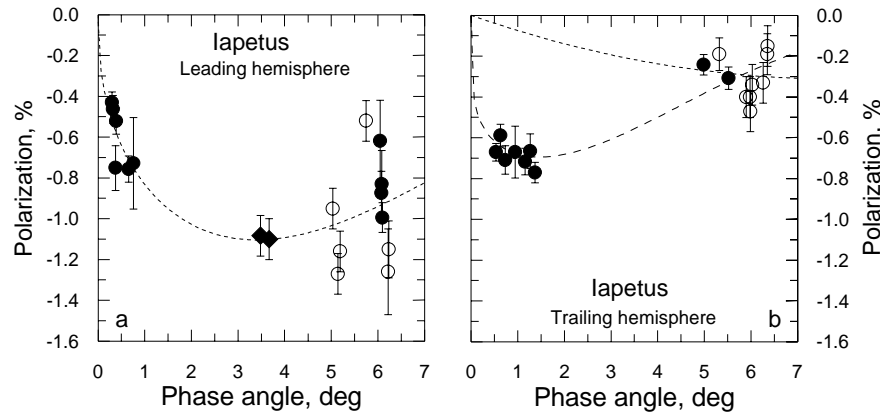


Figure 6: The polarization of the leading (a) and trailing (b) hemispheres of Iapetus in the R filter. Filled circles show data by Rosenbush *et al.* [144]; filled diamonds – those by Jockers [144]; open circles – those by Zellner [146,171].

64 Angelina. During the 1995, 1999, and 2000–2001 oppositions, the UBVR polarimetry of the E-type asteroid 64 *Angelina* was performed with the same equipment as the observations of Iapetus [144,145]. The phase-angle dependence of polarization in different filters clearly shows the presence of the POE in the form of a narrow peak of negative polarization centered at $\alpha \sim 1.5^{\circ}$ and superimposed on the regular negative polarization branch (Fig. 7). The amplitude of the POE is apparition-dependent. Similar apparition dependence of the brightness for *Angelina* had already been noticed by Poutanen [172]. In addition, there is a distinct difference between the POE amplitudes before and after the 1999 opposition. As one can see in Fig. 7, the P_{\min} value of the polarization opposition spike also depends on wavelength. The angular half-width of the polarization spike is comparable to that of the brightness opposition peak [100]. Thus, it appears likely that the polarization spike is a manifestation of the coherent backscattering of sunlight by the *Angelina* surface.

The totality of the observations is consistent with the theory of coherent backscattering. According to this theory, high-albedo particulate surfaces should exhibit a strong and very sharp intensity peak centered at zero phase angle [173]. Furthermore, the narrow BOE should be accompanied by the POE provided that the surface grains are comparable to or smaller than the wavelength [7,170]. All objects for which we have discovered a sharp spike of negative polarization have a high albedo (64 *Angelina* – 0.55; Io – 0.61; Europa – 0.64; Ganymede – 0.42) and show a strong and narrow brightness peak [52,55,100]. In agreement with the

theory, the angular semi-widths and the angular positions of the polarization spikes relative to the exact backscattering direction are comparable to the angular semi-widths of the respective photometric opposition peaks.

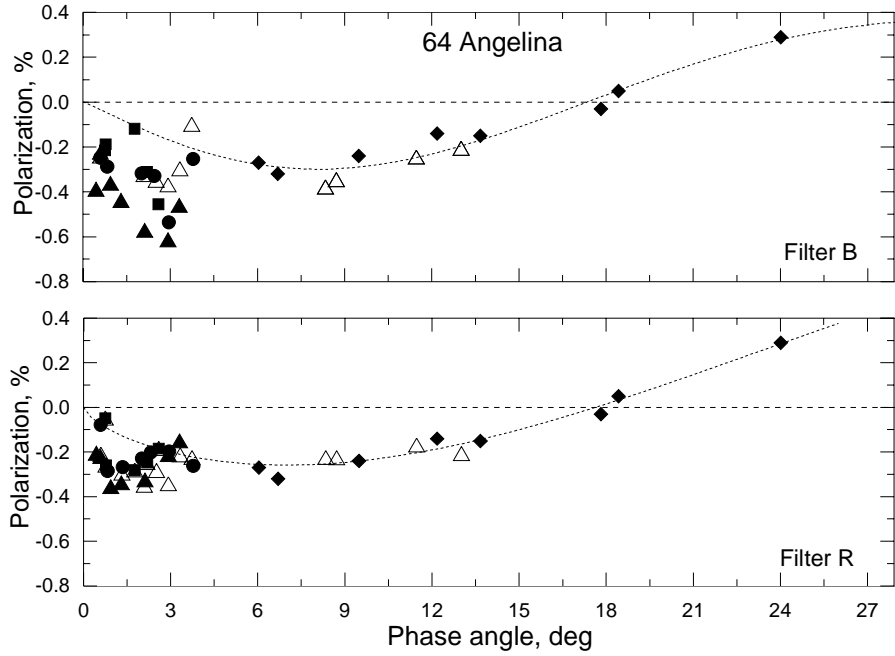


Figure 7: The POE for 64 Angelina in the B and R filters. The dashed curve is a trigonometric polynomial fit to the regular negative polarization branch [57]. Filled circles show the data obtained during the 2000 opposition; filled and open triangles show the data obtained before and after the 1999 opposition, respectively; filled squares show the results collected during the 1995 opposition. Diamonds are the data by Zellner and Gradie [155].

However, the position and amplitude of the observed polarization spikes and the width and amplitude of the brightness peaks can be different for different objects, e.g., for Europa and 64 Angelina. Therefore, it is reasonable to assume that even within the framework of the same optical mechanism (coherent backscattering), the natural variability in particle parameters (such as size, shape, refractive index, porosity) can change the parameters of the BOE and POE.

5. Relationships between photometric and polarimetric opposition effects

Photometric and polarimetric characteristics of light scattered by ASSB surfaces should be interrelated because they are possibly the result of the same optical processes. In particular, it is interesting to study such interrelations in the range of small phase angles, where both the brightness surge and the negative polarization

branch are observed. As follows from the existing theory, two primary physical mechanisms, coherent backscattering and shadow hiding, may explain some of the observed phenomena near opposition. Relative contributions of both mechanisms may depend on the physical properties (composition, porosity, structure, particle sizes, etc.) of the surface layers as well as on the geometry of light scattering. Comparisons of the parameters of the observed photometric and polarization effects may provide some evidence as to what mechanism dominates in specific circumstances.

There are some indications that the BOE and the negative polarization are interrelated. Specifically, Kolokolova [174] found correlations between some parameters of both effects for some ASSBs, but she also pointed out that the number of objects analyzed was not large enough to derive definitive conclusions. A correlation between P_{\min} and the slope of the brightness phase curve at small phase angles for some lunar surface features was detected by Shkuratov [20], who also found indications of a common nature of the negative polarization branch and the BOE. The currently available volume of data sets, including the new polarization data, allows us to revisit this issue.

5.1 Observational data and approximating functions

We have analyzed the entire volume of the available observational data for different objects in order to select objects with a sufficient phase angle coverage and a small scatter of data points in brightness and polarization phase curves. The extrapolation of brightness phase curves to zero phase angle depends on the choice of approximating function and may lead to inaccurate estimates of the BOE parameters. We used a modified four-parameter exponential-linear function by Keränen *et al.* [56]:

$$I_{\text{fit}}(\alpha) = I_s \exp\left(-\frac{\alpha}{1.45 \times \text{HWHM}_B}\right) + I_b + \beta\alpha$$

where I_s is the amplitude of the BOE, I_b is the background intensity, β is the slope of the linear part, and HWHM_B is the semi-width at half-maximum of the BOE. For well-defined phase curves, this function yields the parameters with good accuracy, but it rather strongly depends on the smallest phase angle for which observational data are available. For some objects observed at phase angles down to a few hundredths of a degree (e. g., Europa, Oberon, Titania, Nereid), we have compared the parameters obtained through the exponential-linear fit and directly from observations without any approximation. The agreement is excellent. The main advantage of the exponential-linear fit is that it yields simultaneously all parameters describing the opposition effect and the linear part of the photometric phase curve.

The intensity extrapolated to zero phase angle may be in error because the

detailed shape of the opposition surge in the nearest vicinity of opposition ($\alpha < 1^\circ$) is still unknown for the majority of the objects. The finite angular size of the Sun should be taken into account for such objects as the Moon, Mars, and the satellites of Jupiter and Saturn. The observed photometric phase curves do not form a single family and show significant diversity. For some bodies (e.g., Callisto, Phobos, Deimos), the curvature of the brightness phase dependence changes rather slowly over the entire phase angle range, which does not allow one to identify reliably the linear part. For several dark asteroids (e.g., C- and P-type asteroids), the parameters of the BOE are poorly defined due to the weakness of the opposition surge, and one can see only the linear part of the phase curve.

Table 1 lists the objects analyzed and the disk-integrated or hemisphere-integrated parameters of the BOE: ζ , HWHM_B , β , and α_{opp} . These parameters were also derived for some features of the Europa's, Martian, and lunar surface and are listed in Table 2. The tables also list the corresponding geometric albedo values p_v and provide references to the relevant literature sources. The estimated retrieval errors are as follows: 0.01–0.08 for ζ ; 0.1° – 0.7° for HWHM_B ; 0.0001–0.004 for β ; and 0.1° – 1° for α_{opp} .

In order to determine the parameters of the negative polarization branch P_{min} , α_{min} , and α_{inv} , the observations were fitted with a trigonometric polynomial [57]

$$P_{\text{fit}}(\alpha) = b \sin^{c_1}(\alpha) \cos^{c_2}(\alpha/2) \sin(\alpha - \alpha_{\text{inv}})$$

where the parameters b , c_1 , c_2 , and α_{inv} are determined using a non-linear least-squares fitting technique. The parameter c_2 describes the asymmetry of the polarization phase curve at large phase angles and is usually small, thereby making the term $\cos^{c_2}(\alpha/2)$ close to unity. The disk-integrated or hemisphere-integrated parameters P_{min} , α_{min} , and α_{inv} are listed in Table 3 along with the corresponding values of p_v and HWHM_P and references to the relevant literature sources.

5.2 Correlations between BOE and POE parameters

Figure 8 illustrates the relationships between the BOE parameters ζ , HWHM_B , β , and α_{opp} and the geometric albedo p_v for different ASSBs (the notation is explained in Fig. 9; the letters denote the respective asteroid classes). Two branches on the $\zeta - p_v$ diagram (Fig. 8a) are clearly distinguishable for bright and dark objects. As a consequence, two objects with a very low and a very high albedo may exhibit the same enhancement factor. This is an indication that the BOE for dark and bright objects is likely to be caused by two different optical mechanisms, presumably by the SM and the CBM, respectively. The CBM is a multiple-scattering phenomenon and is more relevant to bright surfaces. On the

Table 1: Parameters of the brightness opposition effect for various ASSBs

| Object | p_v | ζ | HWHM _B deg | β , mag/deg | α_{opp} , deg | Reference |
|--------------------|-------|---------|--------------------------|----------------------|--------------------------------|------------------|
| Moon | 0.12 | 1.63 | 1.11 | 0.0219 | 6.7 | [11,12] |
| Mars | 0.12 | 1.47 | 3.21 | 0.0133 | 16.9 | [37] |
| Phobos | 0.05 | 2.12 | 5.03 | 0.0234 | 14.8 | [42] |
| Deimos | 0.06 | 1.95 | 6.14 | 0.0206 | 17.3 | [42] |
| Io | 0.62 | 1.20 | 0.83 | 0.0235 | 4.7 | [52,175] |
| Europa, leading | 0.68 | 1.14 | 0.30 | 0.0105 | 1.1 | [55] |
| Europa, trailing | 0.68 | 1.27 | 0.16 | 0.0129 | 0.78 | [55] |
| Ganymede, leading | 0.44 | 1.26 | 0.25 | 0.0107 | 1.3 | [52] |
| Callisto, leading | 0.19 | 1.65 | 2.35 | 0.0099 | 12.8 | [55] |
| Callisto, trailing | 0.19 | 1.23 | 1.24 | 0.0255 | 5.4 | [55] |
| Saturn's Ring A | 0.75 | 1.32 | 0.26 | 0.0403 | 1.07 | [89] |
| Saturn's Ring B | 0.82 | 1.27 | 0.31 | 0.0332 | 1.37 | [89] |
| Ring A+B | 0.74 | 1.28 | 0.32 | 0.0368 | 1.22 | [85] |
| Tethys | 0.79 | 1.39 | 0.35 | 0.0157 | 1.6 | [64,66,72,78,79] |
| Iapetus, leading | 0.05 | 1.68 | 2.79 | 0.0115 | 15.2 | [64,65,76,77] |
| Iapetus, trailing | 0.60 | 1.41 | 0.14 | 0.0236 | 0.7 | [64,65,76,77] |
| Hyperion | 0.25 | 1.51 | 0.34 | 0.0096 | 1.8 | [65,70,73] |
| Titania | 0.27 | 1.40 | 0.57 | 0.0210 | 2.2 | [92,93,97] |
| Oberon | 0.23 | 1.58 | 0.47 | 0.0171 | 2.8 | [92,93,97] |
| Nereid | 0.16 | 1.43 | 0.38 | 0.0800 | 1.9 | [95,98] |
| 44 Nysa, type E | 0.55 | 1.28 | 0.80 | 0.0205 | 3.6 | [100] |
| 64 Angelina, E | 0.48 | 1.31 | 0.85 | 0.0198 | 3.9 | [100] |
| 214 Aschera, E | 0.52 | 1.15 | 1.07 | 0.0289 | 4.2 | [107] |
| 317 Roxane, E | 0.49 | 1.22 | 0.72 | 0.0238 | 3.2 | [108] |
| 5 Astraea, S | 0.23 | 1.33 | 2.58 | 0.0257 | 12.0 | [106] |
| 20 Massalia, S | 0.21 | 1.41 | 1.77 | 0.0306 | 8.9 | [99] |
| 29 Amphitrite, S | 0.18 | 1.51 | 2.19 | 0.0242 | 11.3 | [176] |
| 30 Urania, S | 0.17 | 1.72 | 1.85 | 0.0221 | 10.2 | [177] |
| 79 Eurynome, S | 0.26 | 1.50 | 1.37 | 0.0219 | 7.0 | [111] |
| 126 Velleda, S | 0.17 | 1.42 | 0.80 | 0.0267 | 4.0 | [116] |
| 695 Bella, S | 0.16 | 1.22 | 2.20 | 0.0358 | 10.5 | [108] |
| 133 Cyrene, SR | 0.26 | 1.42 | 1.09 | 0.0305 | 5.5 | [103] |
| 16 Psyche, M | 0.10 | 1.58 | 1.61 | 0.0222 | 8.9 | [178] |
| 22 Kalliope, M | 0.14 | 1.43 | 1.68 | 0.0266 | 8.4 | [179] |
| 55 Pandora, M | 0.13 | 1.36 | 1.31 | 0.0297 | 6.3 | [109] |
| 69 Hesperia, M | 0.14 | 1.46 | 2.04 | 0.0247 | 10.2 | [104] |
| 110 Lydia, M | 0.18 | 1.32 | 2.10 | 0.0272 | 10.6 | [180] |
| 201 Penelope, M | 0.16 | 1.49 | 1.99 | 0.0243 | 10.3 | [181] |
| 83 Beatrix, M | 0.09 | 1.40 | 2.26 | 0.0313 | 11.3 | [182] |
| 1 Ceres, G | 0.11 | 1.30 | 1.90 | 0.0395 | 9.4 | [183] |
| 19 Fortuna, G | 0.04 | 1.30 | 3.11 | 0.0271 | 15.3 | [176] |
| 130 Elektra, G | 0.08 | 1.35 | 1.76 | 0.0270 | 9.0 | [111] |
| 10 Hygiea, C | 0.07 | 1.36 | – | 0.0366 | 10 | [112] |
| 47 Aglaja, C | 0.08 | 1.21 | 1.72 | 0.0355 | 7.1 | [158] |
| 165 Loreley, C | 0.08 | 1.22 | 2.52 | 0.0402 | 10.6 | [108] |
| 344 Desiderata, C | 0.04 | 1.19 | 2.50 | 0.0409 | 10.4 | [110] |
| 379 Huena, C? | 0.08 | 1.41 | 0.64 | 0.0404 | 3.4 | [108] |
| 59 Elpis, CP | 0.04 | 1.26 | 3.24 | 0.0398 | 14.3 | [111] |
| 50 Virginia, P | 0.04 | 1.39 | 3.22 | 0.0414 | 16.0 | [184] |
| 102 Miriam, P | 0.05 | 1.26 | 2.46 | 0.0434 | 10.9 | [184] |
| 276 Adelheid, PC | 0.04 | 1.05 | 1.24 | 0.0504 | 4.2 | [110] |

Table 2: Parameters of the brightness opposition effect for some features of the Europa's, Martian, and lunar surfaces

| Object | | p_v | ζ | HWHN _B deg | β , mag/deg | α_{opp} , deg |
|---|------------------|-------|---------|--------------------------|----------------------|--------------------------------|
| Features of the lunar surface [12,15–17,27] | | | | | | |
| Wood's Region | | 0.07 | 5.4 | 0.44 | 0.0142 | 3.5 |
| Platon | | 0.07 | 1.7 | 3.44 | 0.0176 | 18.6 |
| Mare Imbrium | | 0.08 | 2.36 | 0.79 | 0.0176 | 5.1 |
| Sinus Media | | 0.08 | 1.41 | 0.51 | 0.0157 | 3.1 |
| Features of the Martian surface [38,39] | | | | | | |
| Bright areas, | $\lambda 539$ nm | 0.21 | 1.18 | 1.81 | 0.0133 | 7.7 |
| | $\lambda 592$ nm | 0.30 | 1.16 | 0.86 | 0.0120 | 3.5 |
| Flat areas 1, | $\lambda 539$ nm | 0.20 | 1.16 | 1.19 | 0.0144 | 4.8 |
| | $\lambda 592$ nm | 0.29 | 1.15 | 0.77 | 0.0109 | 3.1 |
| Flat areas 2, | $\lambda 592$ nm | 0.29 | 1.10 | 0.30 | 0.0117 | 1.0 |
| Dark areas, | $\lambda 539$ nm | 0.18 | 1.14 | 1.82 | 0.0117 | 7.0 |
| | $\lambda 592$ nm | 0.21 | 1.08 | 1.09 | 0.0064 | 3.5 |
| Crater Tails, | $\lambda 592$ nm | 0.29 | 1.14 | 0.85 | 0.0139 | 9.2 |
| Arabia BR, | $\lambda 592$ nm | 0.34 | 1.14 | 1.29 | 0.0163 | 5.0 |
| Arabia FL, | $\lambda 592$ nm | 0.34 | 1.09 | 0.44 | 0.0266 | 1.4 |
| Syrtis Major, BR, | $\lambda 592$ nm | 0.22 | 1.20 | 1.35 | 0.0009 | 5.8 |
| Syrtis Major FL, | $\lambda 592$ nm | 0.18 | 1.05 | 1.81 | 0.0119 | 4.5 |
| Chryse BR, | $\lambda 592$ nm | 0.30 | 1.15 | 1.03 | 0.0094 | 3.9 |
| Chryse BFL, | $\lambda 592$ nm | 0.29 | 1.14 | 0.49 | 0.0073 | 1.9 |
| Chryse AFL, | $\lambda 592$ nm | 0.29 | 1.12 | 1.09 | 0.0112 | 3.9 |
| Chryse DA, | $\lambda 592$ nm | 0.21 | 1.11 | 1.71 | 0.0039 | 5.8 |
| Mare Erythraeum, | $\lambda 592$ nm | 0.22 | 1.15 | 2.16 | 0.0005 | 8.5 |
| Features of the Europa's surface [63] | | | | | | |
| IR-bright icy | | 0.96 | 1.56 | 0.08 | 0.0340 | 0.50 |
| IR-dark icy | | 0.93 | 1.57 | 0.08 | 0.0332 | 0.48 |
| Dark lineaments | | 0.74 | 1.82 | 0.08 | 0.0217 | 0.49 |
| Dark spot | | 0.48 | 1.68 | 0.09 | 0.0524 | 0.44 |
| Dark ridge | | 0.64 | 1.65 | 0.09 | 0.0242 | 0.51 |
| IR-dark icy ridge | | 0.77 | 1.48 | 0.12 | 0.0220 | 0.63 |

other hand, the SM is a single-scattering phenomenon, and as such is more relevant to dark surfaces. It is, thus, expected that the CBM is stronger for bright surfaces, whereas the SM is stronger for dark surfaces. For all dark objects, with the exception of Phobos, Deimos, and some features on the Moon (see Tables 1 and 2), the values of ζ do not exceed 1.8, whereas for all bright objects $\zeta < 1.6$. These values are in a good quantitative agreement with theoretical predictions [186,173,170].

Low-albedo objects display a great scatter in ζ , which may be attributed to varying porosity of regoliths [186]. For bright objects, the multiple-scattering contribution increases with increasing albedo and raises the enhancement factor, which is in agreement with the theory of the CBM. For moderate-albedo objects ($p_v \approx 0.3$), both the SM and CBM can contribute to the opposition effect. A non-

monotonic dependence of the BOE amplitude on albedo for asteroids, which was found in [115], is only one part of the two-branch dependence for a wide class of objects.

Table 3: Parameters of the negative polarization branch for various ASSBs

| Object | P_{\min} , % | α_{\min} , deg | α_{inv} , deg | HWHM_B , deg | References |
|-----------------------------|-------------------|--------------------------|--------------------------------|--------------------------|------------|
| Whole Moon | -1.3 | 10 | 22.7 | 2.1 | [130] |
| Moon, Mare Imbrium | -1.0 | 11.5 | 23.5 | 3.2 | [130] |
| Mercury | -1.4 | 10 | 25 | | [133] |
| Mars | -1.0 | 12 | 24–29 | | [135] |
| Deimos | -1.5 | 10.3 | 19.5 | 4.0 | [138] |
| Io | -0.21 | 3.5 | 9.7 | 1.0 | [185] |
| Europa | -0.22 | 5.2 | 8.6 | 1.5 | [185] |
| Ganymede | -0.29 | 3.3 | 8.9 | 0.97 | [185] |
| Callisto, leading side | -0.85 | 10.1 | 26 | 1.72 | [60] |
| Callisto, trailing side | -0.63 | 4.9 | 14 | 0.65 | [60] |
| Dione | -0.4 | | | | [141] |
| Rhea | -0.4 | | | | [141] |
| Iapetus, leading side | -1.1 | 3.0 | | 0.36 | This work |
| Iapetus, trailing side | -0.2 | | | | This work |
| Comets | -1.6 | 11.2 | 21.5 | 2.6 | [164] |
| Interplanetary Dust | ≈ -2 | | ≈ 12 | | [167] |
| Saturn's Ring B | -0.38 | 2 | 7 | 0.3 | [151] |
| Asteroids: [160, this work] | | | | | |
| 1 Ceres | -1.71 | 7.2 | 17.8 | 1.68 | |
| 5 Astraea | -0.70 | 8.2 | 19.1 | 2.13 | |
| 16 Psyche | -1.43 | 9.8 | 25.3 | 2.84 | |
| 19 Fortuna | -1.81 | 10.6 | 21.7 | 3.17 | |
| 20 Massalia | -0.64 | 6.7 | 20.1 | 0.73 | |
| 24 Themis | -1.76 | 8.7 | 21.1 | 2.93 | |
| 29 Amphitrite | -0.90 | 10.4 | 21.8 | 4.1 | |
| 30 Urania | -0.80 | 8.7 | 19.7 | 2.57 | |
| 44 Nysa | -0.31 | 5.1 | 17.3 | 0.68 | |
| 47 Aglaja | -1.46 | 8.4 | 17.8 | 2.78 | |
| 55 Pandora | -0.95 | 8.5 | 17.3 | 1.28 | |
| 64 Angelina | -0.32 | 6.3 | 17.6 | 1.13 | |

One of the main characteristics of the BOE is HWHM_B . As shown by Mishchenko in the framework of the CBM theory [187], HWHM_B can depend strongly on the optical properties of the scattering medium. Figure 8b shows that HWHM_B is inversely proportional to the geometric albedo. The CBM is most effective at small phase angles. Therefore, high-albedo objects should have small HWHM_B values, as is indeed observed. For low-albedo bodies, the large scatter of HWHM_B data points occurs due to variations in physical properties of the surface, mainly the porosity and texture. A similar relationship is observed between α_{opp} and p_v (Fig. 8d). It is a consequence of a strong linear correlation between the HWHM_B and the phase angle at which the BOE starts.

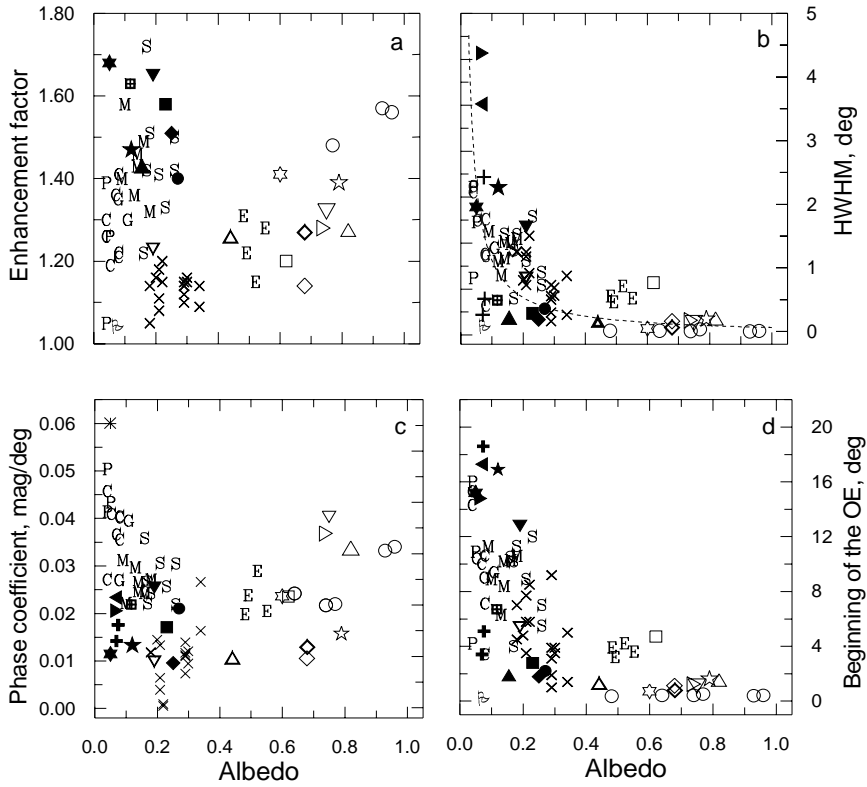


Figure 8: ζ , HWHM_B , β , and α_{opp} versus p_v for a representative selection of ASSBs.

A two-branch dependence of the phase coefficient on the geometric albedo is clearly seen in Fig. 8c. Again, bright and dark objects show different behavior. For low-albedo bodies, the phase coefficient decreases with increasing albedo. Obviously, the growth of the multiple-scattering component results in the attenuation of shadows. For the same reason, high-albedo objects show, in general, lower values of the phase coefficient than low-albedo objects. However, there is an increase of β with increasing albedo for moderate- and high-albedo objects.

If the BOE and the negative polarization have a common origin, then there must be a relationship between the photometric and polarimetric parameters. Indeed, there is a direct correlation between the angular widths of the BOE and POE, as Fig. 10a demonstrates. The bright and dark objects are well separated. Note that the region with $\text{HWHM} \leq 0.5^\circ$ corresponds to objects which exhibit a pronounced opposition spike in brightness and a well-separated negative polarization spike. The region with $0.5^\circ \leq \text{HWHM} \leq 1.5^\circ$ is occupied by bright objects with an opposition spike in brightness and a regular asymmetric negative polarization branch. Low-albedo objects have large angular half-widths, between

1.5° and 3.5°. It is possible that the observed angular half-widths for these objects are the result of simultaneous contributions from the SM and the CBM. Mishchenko [187] showed theoretically that the angular half-width of the coherent opposition effects for silicate surfaces can exceed a few degrees. And indeed, 64 Angelina has the largest values of both HWHM_B and HWHM_P among the high-albedo objects.

| Symbols: | | | |
|-------------------|--------------------|--------------|-----------|
| ■ Moon | □ Io | ▽ Ring A | ● Titania |
| ⊕ Lunar details | ◇ Europa L. | △ Ring B | ■ Oberon |
| ★ Mars | ◊ Europa T. | ▷ Rings A+B | ▲ Nereid |
| ◀ Phobos | ○ European details | ☆ Tethys | * Comets |
| ▶ Deimos | △ Ganymede L. | ★ Iapetus L. | |
| × Martian details | ▼ Callisto L. | ☆ Iapetus T. | |
| | ▽ Callisto T. | ◆ Hyperion | |

Figure 9: Symbols used to denote different objects in Figs. 8 and 10.

The parameters ζ and P_{\min} are essentially the amplitudes of the BOE and the POE, respectively. Unfortunately, the existing theory of coherent backscattering does not predict a well-defined correlation between them. Figure 10b suggests that this relationship can, in fact, be non-monotonic. Additional observations are needed before more definitive conclusions can be reached.

Figure 10c is a scatter plot of α_{\min} versus α_{opp} . A direct correlation between these parameters is rather evident. Furthermore, the objects are obviously segregated into two groups with high and low albedos. Objects exhibiting the POE form a separate group. Figure 10d shows $|P_{\min}|$ versus the geometric albedo. It is evident that $|P_{\min}| \propto 1/p_v$. A very similar dependence was found by Zellner [146].

The dependence of HWHM_B on the wavelength may be a good test of whether CBM can explain the opposition spikes exhibited by high-albedo objects [187–189]. The good agreement between the theoretical and experimental results in Fig. 11 suggests that at least for Saturn’s rings, the opposition brightness spike is undoubtedly caused by coherent backscattering.

6. Summary

Our analyses of the available photometric and polarimetric data collected near opposition lead to the following conclusions.

- Many different classes of ASSBs (planets, satellites, rings, and asteroids as well as cometary and interplanetary dust particles) exhibit a brightness

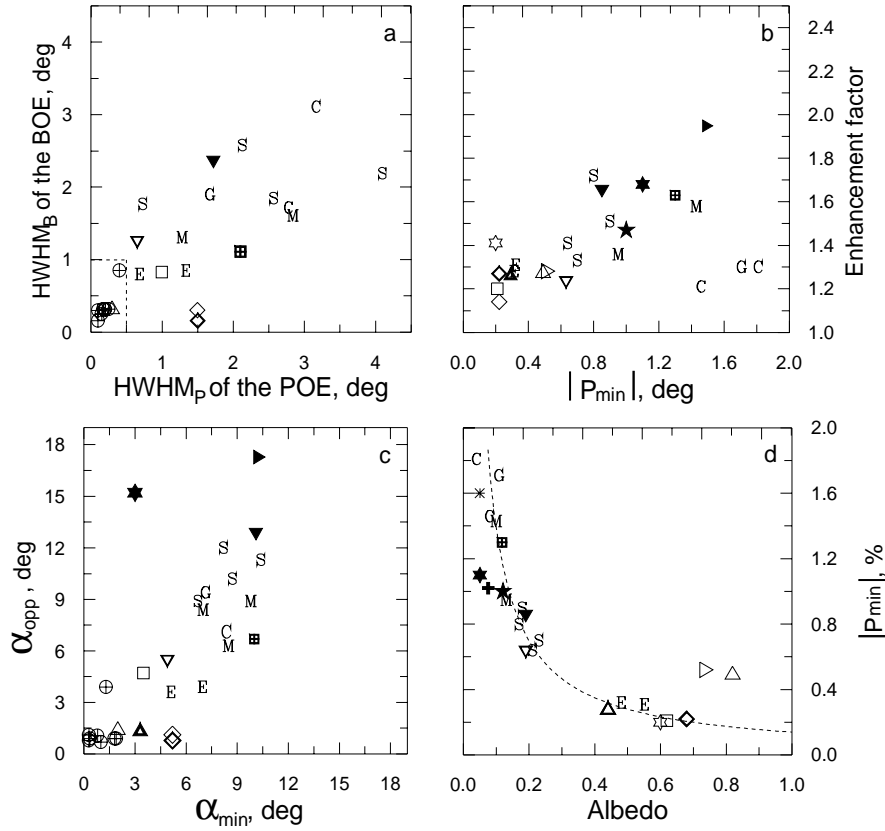


Figure 10: Photometric parameters HWHM_B , ζ , α_{opp} , and p_v versus negative polarization branch parameters HWHM_P , P_{min} , and α_{min} for various ASSBs.

opposition effect and the negative polarization branch at small phase angles. There are significant longitudinal, latitudinal and regional variations in brightness and polarization, which cause peculiarities in the photometric and polarimetric phase curves observed both for entire objects (asteroids, satellites) and for disk-resolved areas (the Moon, Mars, some satellites). The observed photometric phase curves show a great diversity. For some objects (e.g., icy satellites, Saturn's rings, asteroids 44 Nysa and 64 Angelina), a very narrow opposition brightness peak is observed. For some objects (e.g., Callisto, Phobos, Deimos), the curvature of the photometric phase dependence changes rather slowly over a broad range of phase angles, which does not allow one to distinguish a linear part. For some dark objects (e.g., C- and P-type asteroids), the opposition intensity surge is very weak, and one can see only the linear part of the phase curve. These features are related to the physical and chemical properties of the scattering particles.

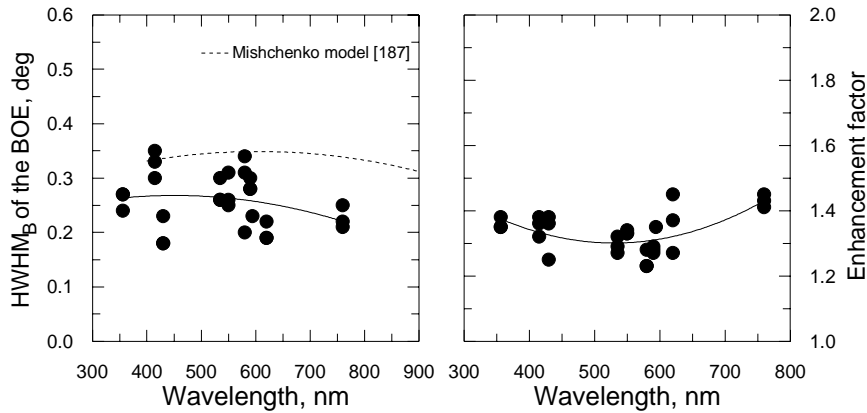


Figure 11: Wavelength dependence of the observed HWHM_B (a) and enhancement factor (b) for Saturn's rings. The dashed curve shows the theoretical dependence of the HWHM_B calculated by Mishchenko [187].

- The shape of the polarization phase curves close to opposition ($\alpha \leq 2^\circ$) was not studied well until quite recently. Our latest observations indicate unambiguously the presence of the POE in the form of a separate peak of negative polarization superimposed on the regular (perhaps slightly asymmetric) negative polarization branch for the Galilean satellites of Jupiter and asteroid 64 Angelina. The lack of observations for the trailing hemisphere of Iapetus does not allow us to determine the shape of the negative polarization branch: it is either highly asymmetric or features a separate peak at very small phase angles. One can expect that the differences in the shape of the polarization minima and their angular locations and amplitudes are caused by varying physical and chemical properties of the scattering particles such as size, refractive index, shape, and porosity. A range of surface types can contribute to the disk-integrated polarization. Therefore, the regular negative polarization branch produced by various kinds of larger grains and/or by surface irregularities can co-exist with the POE peak caused by small grains. Depending on the relative contributions of different mechanisms to the total polarization, the resulting polarization phase curve at small phase angles can vary from object to object.
- The photometric and polarimetric behavior of different ASSBs near opposition is highly variable. The amplitude of the BOE lies in the range 1.1–1.8 in disk-integrated measurements (1.1–5.4 in disk-resolved observations), the half-width at half-maximum varies from 0.7° to 6.1° (from 0.08° to 3.4° in disk-resolved data), the phase angle where the BOE starts varies from 0.7° to 17° (from 0.4° to 19° for disk-resolved features), and the slope of the linear part

varies from 0.01 to 0.06 mag/deg (from 0.0005 to 0.05 mag/deg for disk-resolved features). It should be noted that Phobos and Deimos differ significantly from all other ASSBs studied. The parameters of the negative polarization branch $|P_{\min}|$, α_{\min} , α_{inv} , and HWHM_p are usually in the ranges 0.2 – 2.1%, 2° – 12° , 7° – 29° , and 0.3° – 4° , respectively.

- We have found strong relationships between different parameters of the BOE as well as between the characteristics of the BOE and the negative polarization branch based on a large sample of data for objects with different physical and chemical properties. This result is important because it may suggest the common origin of the photometric and polarization opposition phenomena. Furthermore, these relationships call for an obvious segregation of all ASSBs studied into two groups of high-albedo and low-albedo objects. This result indicates unequivocally the different roles played by the CBM and the SM in the formation of the photometric and polarimetric opposition phenomena for high- and low-albedo objects, respectively.

4. Acknowledgments

We thank Yu. Shkuratov for useful suggestions which improved the manuscript. N. Kiselev and M. Mishchenko appreciate funding from INTAS Grant No. 1999–00652 and the NASA’s Radiation Sciences Program, respectively.

References

1. Yu. Shkuratov, A. Ovcharenko, E. Zubko, *et al.*, *Icarus*, in press (2002).
2. B. Hapke, “Theory of Reflectance and Emittance Spectroscopy” (Cambridge University Press, Cambridge, 1993).
3. Yu. G. Shkuratov, K. Muinonen, E. Bowell, *et al.*, *Earth Moon Planets* **65**, 201 (1994).
4. K. Muinonen, J. Piironen, Yu. G. Shkuratov, *et al.*, in R. Binzel (Ed.), “Asteroids III,” in press (University of Arizona Press, Tucson, AZ, 2002).
5. see chapter by M. Mishchenko, V. Tishkovetz, and P. Litvinov, “Exact Results of the Vector Theory of Coherent Backscattering from Discrete Random Media: An Overview.”
6. B. Lyot, NASA Tech. Transl. F-187 (NASA, Washington, D.C., 1964).
7. M. I. Mishchenko, *Astrophys. J.* **411**, 351 (1993).
8. Yu. G. Shkuratov, *Solar Syst. Res.* **28**, 23 (1994).
9. Yu. G. Shkuratov, *Astron. Vestnik* **25**, 71 (1991).
10. H. N. Russel, *Astrophys. J.* **43**, 103 (1916)
11. G. Rougier, *Ann. L’Obs. Strasbourg* **2**, 205 (1933).
12. T. Gehrels, T. Coffeen, and D. Owings, *Astrophys. J.* **69**, 826 (1964).
13. A. Lane and W. Irvine, *Astron. J.* **78**, 267 (1973).
14. N. P. Barabashev, *Astron. Nachr.* **217**, 445 (1922).
15. V. A. Fedorets, *Uchenye Zapiski Kharkov Univ.* **42**, 49 (1952).

16. R. L. Wildey and H. Pohn, *Astron. J.* **69**, 1964 (1964).
17. J. Van Diggellen, *Planet. Space Sci.* **13**, 271 (1965).
18. K. Peacock, *Icarus* **9**, 16 (1968).
19. W. M. Irvine and A. P. Lane, *Astron. J.* **78**, 267 (1973).
20. Yu. G. Shkuratov, N. V. Opanasenko, and M. A. Kreslavsky, *Icarus* **95**, 283 (1992).
21. B. Hapke, in Z. Kopal (Ed.) "Physics and Astronomy of the Moon," (Academic Press, New York, London, 1971).
22. H. A. Pohn, H. W. Radin, and R. L. Wildey, *Astron. J.* **157**, L193 (1969).
23. H. A. Pohn, R. L. Wildey, and T. W. Offield, NASA SP-272 (1971).
24. R. L. Wildey, NASA SP-315 (1972).
25. S. Nozette et al., *Science* **266**, 1835 (1994).
26. B. J. Buratti, J. K. Hiller, and M. Wang, *Icarus* **124**, 490 (1996) .
27. Yu. Shkuratov, M. Kreslavsky, A. Ovcharenko, et al., *Icarus* **141**, 132 (1999).
28. J. Hiller, B. Buratti, and K. Hill , *Icarus* **141**, 205 (1999) .
29. M. A. Kreslavsky, Yu. G. Shkuratov, Yu. I. Velikodsky, et al., *J. Geophys. Res.* **105**, 20281 (2000).
30. A. Danjon, *Bul. Astron. (Paris)* **14**, 315 (1949).
31. A. Danjon, *Bul. Astron. (Paris)* **17**, 363 (1954).
32. A. Mallama, D. Wang, and R. A. Howard, *Icarus* **155**, 253 (2002).
33. G. Vaucouleurs, *Planet. Space Sci.* **2**, 26 (1959).
34. G. Vaucouleurs, in A. Dollfus (Ed.), "Surfaces and Interiors of Planets and Satellites", p. 267 (Academic Press, London, 1970).
35. B. T. O'Leary, *Astrophys. J.* **149**, L147 (1967).
36. L. A. Bugaenko, I. K. Koval, and A. V. Morozenko, *Astron. Tsirk.* **434** (1976).
37. Yu. V. Aleksandrov, D. F. Lupishko, and T. A. Lupishko, "Absolute Photometry of Mars in 1971, 1973, 1975" (Vishcha Shkola, Kharkiv, 1977).
38. T. E. Thorpe, *Icarus* **37**, 389 (1979).
39. T. E. Thorpe, *Icarus* **47**, 398 (1982).
40. Yu. G. Shkuratov, D. G. Stankevich, A. A. Ovcharenko, et al., *Solar Syst. Res.* **32**, 90 (1998).
41. M. Noland and J. Veverka, *Icarus* **28**, 405 (1976).
42. K. P. Klaasen, T. C. Duxbury, and J. Veverka, *J. Geophys. Res.* **84**, 8478 (1979).
43. J. Veverka and J. A. Burns, *Ann. Rev. Earth Planet. Sci.* **8**, 527 (1980).
44. K. D. Pang, G. W. Rhoads, G. A. Hanover, et al., *J. Geophys. Res.* **88**, 2475 (1983).
45. G. A. Avanesov, B. I. Bonev, F. Kempe, et al., *Nature* **341**, 585 (1989).
46. G. Avanesov, B. Zhukov, Ya. Ziman, et al., *Planet. Space Sci.* **39**, 281 (1991).
47. Yu. G. Shkuratov, N. V. Opanasenko, A. T. Basilevsky, et al., *Planet. Space Sci.* **39**, 341 (1991).
48. B. A. Cantor, M. J. Wolff, P. C. Thomas, et al., *Icarus* **142**, 414 (1999).
49. J. Stebbins, *Lick Obs. Bull.* **13**, 1 (1927).
50. J. Stebbins and T. S. Jacobsen, *Lick Obs. Bull.* **13**, 180 (1928).
51. D. Morrison, N. D. Morrison, and A. R. Lazarewicz, *Icarus* **23**, 399 (1974).
52. R. L. Millis and D. T. Thompson, *Icarus* **26**, 408 (1975).
53. G. W. Lockwood, D. T. Thompson, and K. Lumme, *Astron. J.* **86**, 961 (1980).

54. J. Veverka, in J. A. Burns (Ed.). "Planetary Satellites," p. 171 (University of Arizona Press, Tucson, AZ, 1977).
55. D. T. Thompson and G. W. Lockwood, *J. Geophys. Res.* **97**, 14761 (1992).
56. S. Keränen, K. Muinonen, and J. Piironen, in G. Videen, Q. Fu, and P. Chýlek (Eds.) "Light Scattering by Nonspherical Particles: Halifax Contributions," p. 279 (Army Research Laboratory, Adelphi, MD, 2000).
57. K. Lumme and K. Muinonen, in A. Milani, M. Di Martino, and A. Cellino (Eds.), "Asteroids, Comets, Meteors 1993," p. 194 (Kluwer, Dordrecht, 1993).
58. J. B. Pollack, F. C. Witteborn, E. F. Erickson, D. W. Strecker, B. J. Baldwin, and T. E. Bunch, *Icarus* **36**, 271 (1978).
59. A. L. Line, R. M. Nelson, and D. L. Matson, *Nature* **292**, 38 (1981).
60. V. K. Rosenbush, *Icarus*, in press (2002).
61. D. L. Domingue and A. Verbiscer, *Icarus* **128**, 49 (1997).
62. D. L. Domingue, B. W. Hapke, G.W. Lockwood, and D. T. Thompson, *Icarus* **90**, 30 (1991).
63. P. Helfenstein, N. Currier, B. E. Clark, J. Veverka, et al., *Icarus* **135**, 41 (1998).
64. M. Noland, J. Veverka, D. Morrison, D. P. Cruikshank, et. al., *Icarus* **23**, 334 (1974).
65. F. A. Franklin, and A. F. Cook, *Icarus* **23**, 355 (1974).
66. O. Franz and R. L. Millis, *Icarus* **24**, 433 (1975).
67. B. J. Buratti and J. Veverka, *Icarus* **58**, 254 (1984).
68. B. J. Buratti, *Icarus* **59**, 395 (1984).
69. S. W. Squyres, B. Buratti, J. Veverka, and C. Sagan, *Icarus* **59**, 426 (1984).
70. D. J. Tholen and B. Zellner, *Icarus* **58**, 246 (1984).
71. R. Thomas and J. Veverka, *Icarus* **64**, 414 (1985).
72. B. J. Buratti, J. A. Mosher, and T.V. Johnson, *Icarus* **87**, 339 (1990).
73. J. Degewij, L. E. Andersson, and B. Zellner, *Icarus* **44**, 520 (1980).
74. D. J. Tholen and B. Zellner, *Icarus* **53**, 341 (1983).
75. J. Goguen, H. Hammel, D. P. Cruikshank, and W. K. Hartmann, *Bull. Am. Astron. Soc.* **15**, 854 (1983).
76. R. L. Millis, *Icarus* **31**, 81 (1977).
77. R. W. Payne, *J. British Astron. Ass.* **81**, 123 (1971).
78. G. N. Blair and N. F. Owen, *Icarus* **22**, 224 (1974).
79. C. Blanco and S. Catalano, *Astron. Astrophys.* **33**, 105 (1974).
80. G. Müller, *Publ. Obs. Potsdam* **8**, 193 (1893).
81. H. Seeliger, *Abh. Bayer. Akad. Wiss. Math. Naturwiss. Kl. II*, **18**, 1 (1887).
82. E. Schönberg, *Ann. Acad. Sci. Fennicae Ser. A*, **16**, 5 (1922).
83. E. Hertzsprung, *Astron. Nachr.* **208**, 81 (1919).
84. E. Schönberg, *Vierteljahrsschrift der Astronomischen Gesellschaft* **68**, 387 (1933).
85. F. A. Franklin and A. F. Cook, *Astron. J.* **70**, 704 (1965).
86. K. Lumme and W. M. Irvin, *Astron. J.* **81**, 865 (1976).
87. L. W. Esposito and K. Lumme, *Icarus* **31**, 157 (1977).
88. K. Lumme, L. W. Esposito, W. D. Benton, and W. A. Baum, *Astron. J.* **84**, 1402 (1979).
89. L. W. Esposito, K. Lumme, W. D. Benton, and L. J. Martin, *Astron. J.* **84**, 1408 (1979).

90. W. T. Thompson, K. Lumme, W. M. Irvin, et al., *Icarus* **46**, 187 (1981).
91. R. H. Brown and D. R. Cruikshank, *Icarus* **55**, 83 (1983).
92. J. D. Goguen and H. B. Hammel, *Icarus* **77**, 239 (1989).
93. J. Veverka, P. Thomas, P. Helfenstein, et al., *J. Geophys. Res.* **92**, 14895 (1987).
94. B. Buratti, F. Wong, and J. Mosher, *Icarus* **84**, 203 (1990).
95. B. E. Schaefer and S. W. Tourtellotte, *Icarus* **151**, 112 (2001).
96. E. Karkoschka, *Icarus* **125**, 348 (1997).
97. E. Karkoschka, *Icarus* **151**, 51 (2001).
98. B. E. Schaefer and M. W. Schaefer, *Icarus* **146**, 541 (2000).
99. T. Gehrels, *Astrophys. J.* **123**, 331 (1956).
100. A. W. Harris, J. W. Young, L. Contreiras, et al. *Icarus* **81**, 365 (1989).
101. A. W. Harris and J. W. Young, *Lunar Planet Sci. Conf. XIX* **2**, 447 (1989).
102. A. W. Harris and J. W. Young, *Icarus* **54**, 59 (1983).
103. A. W. Harris, M. Carlsson, J. W. Young, and C.-I. Lagerkvist, *Icarus* **58**, 377 (1984).
104. M. Poutanen, E. Bowell, L. J. Martin, and D. T. Thompson, *Astron. Astrophys. Suppl.* **61**, 291 (1985).
105. A. W. Harris, J. W. Young, E. Bowell, et al. *Icarus* **77**, 171 (1989).
106. C.-I. Lagerkvist, P. Magnusson, I. P. Williams, et al. *Astron. Astrophys. Suppl.* **78**, 519 (1989).
107. C.-I. Lagerkvist and P. Magnusson, *Astron. Astrophys. Suppl.* **86**, 119 (1990).
108. A. W. Harris, J. W. Young, T. Dockweiler, et al., *Icarus* **95**, 115 (1992).
109. V. G. Shevchenko, Yu. N. Krugly, D. F. Lupishko, et al., *Astron. Vestnik* **27**, 75 (1993).
110. J. Piironen, E. Bowell, A. Erikson, and P. Magnusson, *Astron. Astrophys. Suppl.* **106**, 587 (1994).
111. V. G. Shevchenko, V. G. Chorny, and A. V. Kalashnikov, *Astron. Astrophys. Suppl.* **115**, 1 (1996).
112. V. G. Shevchenko, *Solar Syst. Res.* **31**, 219 (1997).
113. L. M. French, *Bull. Am. Astron. Soc.* **19**, 850 (1987).
114. V. G. Shevchenko and D. F. Lupishko, *Solar Syst. Res.* **32**, 250 (1998).
115. I. N. Belskaya and V. G. Shevchenko, *Icarus* **147**, 94 (2000).
116. A. N. Dovgopool, Yu. N. Krugly, and V. G. Shevchenko, *Acta. Astron.* **42**, 67 (1992).
117. D. F. Lupishko and M. Di Martino, *Planet. Space Sci.* **46**, 47 (1998).
118. Yu. G. Krugly and V. G. Shevchenko, *Lunar Planet Sci. Conf. XXX*, 1595 (1999).
119. W. Z. Wisniewski, M. A. Barucci, M. Fulchignoni, et al. *Icarus* **101**, 213 (1993).
120. C. E. Delahodde, K. J. Meech, O. R. Hainaut, and E. Dotto, *Astron. Astrophys.* **376**, 672 (2001).
121. K. J. Meech and D. C. Jewitt, *Astron. Astrophys.* **187**, 585 (1987).
122. D. G. Schleicher, R. L. Millis, and P. V. Birch, *Icarus* **132**, 397 (1998).
123. Y. R. Fernandez, C. M. Lisse, H. U. Kaufl, et al., *Icarus* **147**, 145 (2000).
124. R. Dumont and F. Sanchez, *Astron. Astrophys.* **51**, 393 (1976).
125. J. B. Renard, R. Dumond, and A. C. Levasseur-Regourd, *Astron. Astrophys.* **304**, 602 (1995).
126. A. C. Levasseur-Regourd, J. B. Renard, and R. Dumond, in A. C. Levasseur-Regourd and H. Hasegawa (Eds.), "Origin and Evolution of Interplanetary Dust," p. 191 (Kluwer, Tokyo, 1991).
127. P. L. Lamy and J.-M. Perrin, *Astron. Astrophys.* **163**, 269 (1986).

128. G. V. Coyne and S. F. Pellicori, *Astron. J.* **75**, 54 (1970).
129. A. Dollfus and E. Bowell, *Astron. Astrophys.* **10**, 29 (1971).
130. O. I. Kvartskhelia, *Bull. Abastumani Astrophys. Obs.* **64**, 3 (1988).
131. N. V. Opanasenko and Yu. G. Shkuratov, *Solar Syst. Res.* **28**, 233 (1994).
132. B. Lyot, *C. R. Acad. Sci.* **20**, (1930).
133. A. Dollfus and M. Auriete, *Icarus* **23**, 465 (1974).
134. A. Dollfus, in G. P. Kuiper and B. M. Middlehurst (Eds.), "Planets and Satellites," p. 306 (University of Chicago Press, Chicago, IL, 1961).
135. A. Dollfus and J. Focas, *Astron. Astrophys.* **2**, 63 (1969).
136. A. V. Morozhenko, *Astron. Zh.* **50**, 1057 (1973).
137. O. I. Bugaenko, A. V. Morozhenko, and E. G. Yanovitskij, in T. Gehrels (Ed.), "Planets, Stars, and Nebulae Studied with Photopolarimetry," p. 599 (University of Arizona Press, Tucson, AZ, 1974).
138. B. Zellner, *Astron. J.* **77**, 183 (1972).
139. J. Veverka, *Icarus* **14**, 355 (1971).
140. A. Dollfus, *Icarus* **25**, 416 (1975).
141. J. Veverka, in J. A. Burns (Ed.), "Planetary satellites," p. 210 (University of Arizona Press, Tucson, AZ, 1977).
142. R. A. Chigladze, PhD thesis, Abastumany Astrophys. Obs. (1989).
143. V. K. Rosenbush, V. V. Avramchuk, A. E. Rosenbush, and M. I. Mishchenko, *Astrophys. J.* **487**, 402 (1997).
144. V. K. Rosenbush, N. N. Kiselev, K. Jockers, et al., *Kinem. Phys. Celest. Bodies. Suppl. Ser. No.* **3**, 227 (2000).
145. V. K. Rosenbush, N. N. Kiselev, V. V. Avramchuk, et al., in B. Gustafson, L. Kolokolova, and G. Videen (Eds.), "Electromagnetics and Light Scattering by Nonspherical Particles," p. 279 (Army Research Laboratory, Adelphi, MD, 2002).
146. B. Zellner, *Astrophys. J.* **174**, L107 (1972).
147. E. Bowell and B. Zellner, in T. Gehrels (Ed.), "Planets, Stars, and Nebulae Studied with Photopolarimetry," p. 381 (University of Arizona Press, Tucson, AZ, 1974).
148. J. C. Kemp and R. E. Murphy, *Astrophys. J.* **189**, 679 (1973).
149. A. Dollfus, *Icarus* **37**, 404 (1979).
150. P. E. Johnson, J. C. Kemp, R. King, et al., *Nature* **283**, 146 (1980).
151. A. Dollfus, *Icarus* **124**, 96 (1996).
152. B. Lyot, *C. R. Acad. Sci.* **199**, 774 (1934).
153. B. Zellner and J. Gradie, *Icarus* **28**, 117 (1974).
154. B. Zellner, T. Gehrels, and J. Gradie, *Astron. J.* **79**, 1100 (1974).
155. B. Zellner and J. Gradie, *Astron. J.* **81**, 262 (1976).
156. A. Dollfus, M. Wolf, J. E. Geake, et al., in M. P. Binzel, T. Gehrels, and M. S. Matthews (Eds.), "Asteroids-II," p. 594 (University of Arizona Press, Tucson, AZ, 1989).
157. D. F. Lupishko, Doctoral thesis, Kharkiv Univ. (1999).
158. G. P. Chernova, D. F. Lupishko, V. G. Shevchenko, et al., *Kinem. Phys. Celest. Bodies* **7**, 20 (1991).

159. D. F. Lupishko, N. N. Kiselev, and G. P. Chernova, *Kinem. Phys. Celest. Bodies* **10**, 40 (1994).
160. D. F. Lupishko and C. B. Vasilyev, *Kinem. Phys. Celest. Bodies* **13**, 17 (1997) (<http://pdssbn.astro.umd.edu/sbnhtml/>).
161. I. N. Belskaya, N. N. Kiselev, N. M. Shakhovskoj, et al., in "Abstracts: Asteroids, Comets, Meteors," p. 59 (Cornell University, Ithaca, NY, 1999).
162. N. N. Kiselev and G. P. Chernova, *Sov. Astron.* **22**, 607 (1978).
163. N. N. Kiselev and G. P. Chernova, *Icarus* **48**, 473 (1981).
164. G. P. Chernova, N. N. Kiselev, and K. Jockers, *Icarus* **103**, 144 (1993).
165. N. N. Kiselev, N. M. Shakhovskoy, and Yu. S. Efimov, *Icarus* **120**, 408 (1996).
166. R. D. Wolstencroft and L. J. Rose, *Astrophys. J.* **147**, 271 (1967).
167. A. C. Levasseur-Regourd, R. Dumond, and J. B. Renard, *Icarus* **86**, 264 (1990).
168. A. C. Levasseur-Regourd, J. B. Renard, and R. Dumond, in A. C. Levasseur-Regourd and H. Hasegawa (Eds.), "Origin and Evolution of Interplanetary Dust," p. 191 (Kluwer, Tokyo, 1991).
169. V. V. Korokhin, S. A. Beletsky, Yu. I. Velikodsky et al., *Kinem. Phys. Celest. Bodies* **16**, 80 (2000).
170. M. I. Mishchenko, J.-M. Luck, and T. M., Nieuwenhuizen, *J. Opt. Soc. Am. A* **17**, 888.
171. J. Veverka, in J. A. Burns (Ed.), "Planetary Satellites," p. 244 (University of Arizona Press, Tucson, AZ, 1977).
172. M. Poutanen, in C.-I. Lagerkvist and H. Rickman (Eds.), "Asteroids, Comets, Meteors," p. 45 (Uppsala University, Uppsala, 1983).
173. M. I. Mishchenko and J. M. Dlugach, *Mon. Not. Royal Astron. Soc.* **254**, 15P (1992); M. I. Mishchenko and J. M. Dlugach, *Planet. Space Sci.* **41**, 173 (1993).
174. O. Kolokolova, in A. V. Morozhenko (Ed.), "Photometric and Polarimetric Investigations of Celestial Bodies," p. 38 (Naukova Dumka, Kyiv, 1985).
175. D. Morrison and N. D. Morrison, in J. A. Burns (Ed.), "Planetary Satellites," p. 363 (University of Arizona Press, Tucson, AZ, 1977).
176. D. F. Lupishko, F. A. Tupieva, F. P. Velichko, et al., *Astron. Vestnik* **15**, 25 (1981).
177. W. Z. Wisniewski, T. M. Michowski, A. W. Harris, and R. S. McMillan, *Icarus* **126**, 395 (1997).
178. E. F. Tedesco, R. C. Taylor, J. Drummond, et al., *Icarus* **54**, 30 (1983).
179. F. Scaltriti, V. Zappala, and R. Stanzel, *Icarus* **34**, 93 (1978).
180. R. C. Taylor, T. Gehrels, and A. B. Silvester, *Astron. J.* **76**, 141 (1971).
181. V. G. Shevchenko, PhD thesis, Kharkiv University (1997).
182. C.-I. Lagerkvist and P. Magnusson, *Astron. Astrophys. Suppl.* **108**, 143 (1994).
183. E. F. Tedesco, R. C. Taylor, J. Drummond, et al., *Icarus* **54**, 23 (1983).
184. V. G. Shevchenko, I. N. Belskaya, V. G. Chiorny, et al., *Planet. Space Sci.* **45**, 1615 (1997).
185. V. K. Rosenbush, V. V. Avramchuk, *Astron. Vestnik* **33**, 307 (1999).
186. B. Hapke, *Icarus* **67**, 264 (1986).
187. M. I. Mishchenko, *Astrophys. Space Sci.* **194**, 327 (1992).
188. B. Hapke, R. Nelson, and W. Smithe, *Icarus* **133**, 89 (1998).